Mon. Not. R. Astron. Soc. **000**, 000–000 (0000) Printed 7 February 2008 (MN LATEX style file v2.2)

Rotating neutron stars: an invariant comparison of approximate and numerical spacetime models

Emanuele Berti[1], Frances White[2], Asimina Maniopoulou[3], Marco Bruni[2]
[1] *McDonnell Center for the Space Sciences, Department of Physics, Washington University, St. Louis, Missouri 63130, USA. Present address: Groupe de Cosmologie et Gravitation (GReCO), Institut d'Astrophysique de Paris (CNRS), 98bis Boulevard Arago, 75014 Paris, France*
[2] *Institute of Cosmology and Gravitation, Mercantile House, Hampshire Terrace, University of Portsmouth, Portsmouth PO1 2EG, UK*
[3] *School of Mathematics, University of Southampton, Southampton SO17 1BJ, UK*

7 February 2008

ABSTRACT

We compare three different models of rotating neutron star spacetimes: i) the Hartle-Thorne (1968) slow-rotation approximation, keeping terms up to second order in the stellar angular velocity; ii) the exact analytic vacuum solution of Manko *et al.* (2000a, 2000b); and iii) a numerical solution of the full Einstein equations. In the first part of the paper we estimate the limits of validity of the slow-rotation expansion by computing relative errors in the spacetime's quadrupole moment Q and in the corotating and counterrotating radii of Innermost Stable Circular Orbits (ISCOs) $R_{\pm}$. We integrate the Hartle-Thorne structure equations for five representative equations of state. Then we match these models to numerical solutions of the Einstein equations, imposing the condition that the gravitational mass and angular momentum of the models be the same. We find that the Hartle-Thorne approximation gives very good predictions for the ISCO radii, with $R_{\pm}$ accurate to better than 1% even for the fastest millisecond pulsars. At these rotational rates the accuracy on Q is $\sim 20\%$, and better for longer periods. In the second part of the paper we focus on the exterior vacuum spacetimes, comparing the Hartle-Thorne approximation and the Manko analytic solution to the numerical models using Newman-Penrose (NP) coordinate-independent quantities. For all three spacetimes we introduce a physically motivated 'quasi-Kinnersley' NP frame. In this frame we evaluate a quantity, the speciality index S, measuring the deviation of each stellar model from Petrov Type D. Deviations from speciality on the equatorial plane are smaller than 5% at star radii for the faster rotating models, and rapidly decrease for slower rotation rates and with distance. We find that, at leading order, the deviation from Type D is proportional to $(Q - Q_{\rm Kerr})$. Our main conclusion is that the Hartle-Thorne approximation is very reliable for most astrophysical applications.

Key words: stars: relativity — stars: neutron — stars: rotation

1 INTRODUCTION

Pulsars are observed to rotate with periods as small as 1.56 ms (Backer *et al.* 1982, Kulkarni 1995, Chakrabarty *et al.* 2003). Fast rotation is also very important in newly-born neutron stars, which may undergo secular and dynamical instabilities (Andersson & Kokkotas 2001, Kokkotas & Ruoff 2002). An accurate modelling of the spacetime of rotating stars is therefore important both in astrophysical studies and in investigations of sources of gravitational waves. The aim of this paper is to compare two relativistic approximate models, the slow rotation expansion of Hartle & Thorne (1968, henceforth HT) and the exact vacuum solution by Manko *et al.* (Manko 2000a, 2000b), with a full general-relativistic numerical one, quantifying the range of validity of the HT expansion and studying the possible overlap of the two approximations.

The Schwarzschild metric describes either a non-rotating black hole (BH) or the exterior of a non-rotating star: this is a well-known consequence of Birkhoff's theorem. In contrast, the rotating Kerr BH metric describes a rotating star only to linear order in rotational velocity. At higher orders, the multipole moments of the gravitational field created by a rapidly rotating compact star differ from those of a BH. This difference in the multipolar structure

has important consequences for the observation of the electromagnetic and gravitational radiation from these objects. For example, the detection of gravitational waves emitted by particles in orbit around BHs and compact stars can be used, in principle, to map the multipolar structure of the corresponding spacetime and check the validity of the BH no-hair theorem (Ryan 1995, 1997; Collins & Hughes 2004).

A relatively simple description of the spacetime of rotating stars was developed many years ago by Hartle and collaborators (Hartle 1967, Hartle & Thorne 1968; see also Chandrasekhar & Miller 1974) using a slow rotation expansion, that is, an expansion in the parameter $\epsilon = \Omega/\Omega^*$. Here Ω is the star's angular velocity and $\Omega^* = (M/R^3)^{1/2}$ is a rotational scale set by the Keplerian frequency of a test particle sitting on the equator of a non-rotating star with gravitational mass M and radius R (throughout this paper we use geometrical units, $G = c = 1$). In the Newtonian limit, uniformly rotating polytropic stars shed matter at the equator at a mass-shedding frequency which is roughly given by $\Omega_K \simeq (2/3)^{3/2}\Omega^*$. This is not true in a general relativistic framework (see eg. Stergioulas 2003). However Ω^* does give an order of magnitude estimate of the mass shedding frequency, so we can roughly expect the HT treatment to break down when $\epsilon \sim 1$.

The HT method allows a systematic computation of the interior and exterior structure at successive orders in ϵ. At order ϵ, deviations from non-rotating stellar models are due to the relativistic frame dragging, but the stellar structure is still spherical. Deviations from sphericity are measured by the star's quadrupole moment; they appear at order ϵ^2. Being a slow-rotation expansion, the HT metric is expected to lose accuracy for rapid spin rates, but the limits of validity of the approximation are not well understood. Weber & Glendenning (1992) compared the slow-rotation expansion with early numerical results by Friedman *et al.* (1986). Their comparison led to 'compatible results' down to rotational Kepler periods $P_K \simeq 0.5$ ms. However their self-consistency equation [Eq. (7) in Weber & Glendenning (1992)] to determine the mass-shedding frequency is not consistently truncated at second order in angular velocity, as it should be. This is presumably one of the reasons their method becomes very inaccurate close to the limiting-mass model.

Numerical solutions for uniformly rotating stars can now be obtained in both the slow and fast-rotation regimes. The HT approximation is quite simple to implement: our own numerical code will be described in Section 3. In contrast, a solution of the Einstein equations for rapidly rotating models is non-trivial. Komatsu, Eriguchi and Hachisu (1989) devised a self-consistent method to solve the full Einstein equations, which was later improved by Cook, Shapiro and Teukolsky (1994, henceforth CST). Stergioulas' RNS code (Stergioulas & Friedman 1995) is a variant of the CST code which has been extended to allow for strange-star matter equations of state (EOSs), differential rotation, computation of multipole moments and so on. A very accurate spectral method for computing rapidly rotating stellar models was independently developed by Bonazzola *et al.* (cf. Bonazzola *et al.* 1993, Salgado *et al.* 1994) and became part of the numerical relativity library LORENE (Bonazzola *et al.* 1998). Nozawa *et al.* (1998) showed that the different numerical methods are in remarkable agreement, typical differences being of order 10^{-3} or smaller for smooth EOSs. A new multi-domain spectral method has been introduced by Ansorg *et al.* (2002), who achieved near-machine accuracy for uniform density stars; their results are in very good agreement with those of the other groups. The RNS code therefore provides a numerically accurate description of fast-rotating relativistic stars.

Berti & Stergioulas (2003, henceforth BS) used the RNS code to compute constant rest-mass (so-called evolutionary) sequences of three types using five realistic EOSs. The first type mimics the evolutionary track of a canonical neutron star having gravitational mass $M = 1.4M_\odot$ in the non-rotating limit. The second type has the maximum gravitational mass $M = M_{\rm max}$ allowed by the given EOS in the non-rotating limit. In the following, we will sometimes refer to these sequences as type '14' and type 'MM'. The third type is supramassive: its baryon mass is larger than allowed by the non-rotating Tolman-Oppenheimer-Volkoff (TOV) equations. A supramassive sequence does not terminate with a non-rotating model, so that a comparison with HT models is not always possible. Therefore we do not consider supramassive models in the following.

Another method of approximating the exterior spacetime takes the form of a multipole expansion far from the star. This technique has been used by Shibata & Sasaki (1998) to derive approximate analytic expressions for the location of the Innermost Stable Circular Orbits (ISCOs) around rapidly rotating relativistic stars. However the technique cannot easily be applied to other problems. Furthermore, the relevant multipole moments must be computed *numerically* for each model one wants to analyze, and then plugged into the relevant formulas.

Approximate analytic models for fast rotating stars which include only the most relevant multipolar structure of the exterior spacetime (that is, the lowest-order mass and current multipoles) would be very useful for astrophysical applications. In this paper we focus on an interesting family of solutions found by Manko *et al.* (2000a, 2000b). They used Sibgatullin's method (Sibgatullin 1991), which has the advantage that the multipolar structure of the spacetime can be prescribed *a priori*, to find an exact, nine-parameter, analytic solution of the Einstein-Maxwell equations. Consideration of the full Einstein-Maxwell system is motivated by the fact that compact stars normally have extremely large magnetic fields, which could significantly change their properties (Bocquet *et al.* 1995) and the development of instabilities (Spruit *et al.* 1999; Rezzolla *et al.* 2000). However, for simplicity, we do not consider effects due to magnetic fields in this paper.

An approximate description of a rapidly rotating neutron star can be obtained using a five parameter sub-case of the analytic solution (Manko 2000b). Ignoring charge and magnetic moment the free parameters reduce to three. This three-parameter solution is an *exact* solution of the Einstein equations in vacuum, but it only provides an approximate description of a neutron star exterior[1].

[1] BS focused on four out of the *a priori* infinite multipole moments of the Manko metric: gravitational mass M, angular momentum J, mass quadrupole moment Q and current octupole moment S_3. However their statement that these are the only nonvanishing moments is not precise: there do exist higher-order nonvanishing physical moments of the Manko metric.

BS showed that the Manko solution approximates rather well the field of a rapidly rotating neutron star in the fast rotation regime. They used the three parameters of the analytic solution to match the dominant multipole moments (M, J and $M_2 = -Q$) to given numerical models. They found that an indicative measure of the deviation of the Manko metric from the numerical metric is given by the relative error in the first non-freely adjustable multipole moment: the current octupole S_3. BS found a peculiar feature of the Manko solution: the solution's quadrupole moment *cannot* be matched to the quadrupole moment of numerically computed spacetimes for slow rotation rates. Therefore, it is of interest to understand whether the regimes where the HT and the Manko metrics are applicable are completely distinct, or have some range of Ω in common.

This paper compares the HT slow rotation expansion and the exact vacuum solution by Manko *et al.* with the full general-relativistic numerical CST spacetime. We will assume that our numerical models, obtained using the RNS code, are *exact* (within their numerical accuracy, that is of the order of 10^{-4} in each computed quantity). An overview of the three different spacetimes we consider in this paper is presented in Section 2, where we also introduce our notation.

The rest of the paper consists of two parts. In the first we integrate the HT equations of structure for the same set of 'realistic', nuclear physics motivated EOSs examined in BS (Section 3). From the stable models in the HT sequence we choose those which have the same gravitational mass and angular momentum as a given numerical model. The procedure to do this is developed in Section 3.1.

In Section 4 we quantify deviations of the HT and CST spacetimes. A trustworthy measure of the deviation is given by the relative error in the first non-freely adjustable multipole moment in the HT spacetime: $M_2 = -Q$. Picking a representative EOS we show that deviations in Q are at most $\sim 20\%$ at the rotation rates corresponding to the fastest observed millisecond pulsar PSR J1939+2134 (Backer *et al.* 1982), for both mass sequences. We also use some recent results by Abramowicz *et al.* (2003) to compute the ISCO radii predicted by the HT approximation for sequences of slowly-rotating models. We find an interesting result: the HT approximation gives *an excellent approximation to the ISCO predicted by numerical solutions*, relative errors being smaller than 1 % for astrophysically relevant rotation rates, down to the 1.5 ms period of PSR J1939+2134.

In the second part of the paper we compare the three vacuum exterior spacetimes, focusing on invariant quantities, and looking at their Petrov classification. In a nutshell, the Petrov classification of a spacetime depends on which of the Weyl scalars can be set to zero by suitable tetrad rotations (Chandrasekhar 1983, Stephani *et al.* 2003, Stephani 2004). The Kerr metric is of Petrov Type D, hence algebraically special. In general, rotating perfect fluid spacetimes will *not* be of Type D (see eg. Fodor and Perjès 2000), but will be of (general) Type I. Our invariant comparison of the three different models involves quantifying the deviation of each metric from speciality. Indeed one might wish to assume (for example in perturbative calculations of gravitational wave emission) that rotating neutron star spacetimes are in some sense 'close' to Type D. Then one should develop a tool to quantify their 'non-Type-D-ness': here we use the curvature invariant speciality index S introduced by Baker & Campanelli (2000). Each metric is expressed in different coordinates, so we evaluate S at the stellar radius, a physically identifiable radial location. This quantity may also indicate whether it is sensible to carry out perturbative calculations on neutron star backgrounds in a 'Type-D-approximation', and to extract the gravitational wave content of the spacetime through a Teukolsky-like formalism. In this paper, however, we will focus only on calculations of the Weyl scalars in the background spacetimes.

We choose the simplest and most physically transparent tetrad to compute the Weyl scalars and to characterise the non-Type-D-ness of the spacetime. First of all we construct a transverse tetrad, in which $\psi_1 = \psi_3 = 0$, so getting rid of this tetrad gauge freedom (Szekeres 1965). Then we carry out a tetrad rotation to go to the canonical frame in which $\psi_0 = \psi_4 \equiv \psi_{04}$ (Pollney *et al.* 2000; Re *et al.* 2003), that we call symmetric. In a Type I spacetime, there are three distinct equivalence classes of transverse frames (Beetle & Burko 2002), each containing a symmetric tetrad. From these three different symmetric tetrads we select a 'quasi-Kinnersley' tetrad (cf. Nerozzi *et al.* 2004), i.e. the one that directly reduces to the canonical frame for Type D when we set the parameters to reduce the metric to this type.

We apply this procedure, which is described in detail in Section 5, to all three metrics. In Section 6 we show the scalars and the corresponding speciality index. We find that deviations from speciality on the equatorial plane are smaller than 5% at the stellar radius, even for the faster rotating models. These deviations rapidly decrease for slower rotation rates and at larger distances from the star. We find that, at leading order, the deviation from Type D is proportional to $(Q - Q_{\rm Kerr})$. The conclusions and a discussion follow.

2 THE THREE METRICS

The three metrics we will consider in this paper (HT, Manko and CST) can be written in the following general axisymmetric stationary form, with coordinates $[t, c_1, c_2, \phi]$

$$ds^2 = g_{00}dt^2 + 2g_{03}dtd\phi + g_{33}d\phi^2 + g_{11}dc_1^2 + g_{22}dc_2^2 \quad (1)$$

where all the metric coefficients are functions of c_1 and c_2 only. Being stationary and axisymmetric the spacetime has two Killing vectors, one timelike $\xi^a = [1, 0, 0, 0]$ and one spacelike $\varphi^a = [0, 0, 0, 1]$.

The metrics can be explicitly written as:

$$\begin{aligned}(ds^2)_{HT} &= -e^{\nu}(1+2h)dt^2 + e^{\lambda}[1+2m/(r-2M)]dr^2 \\ &\quad + r^2(1+2k)[d\theta^2 + \sin^2\theta(d\phi - \omega dt)^2] \end{aligned} \quad (2)$$

$$\begin{aligned}(ds^2)_{Manko} &= f^{-1}[e^{2\gamma}(d\rho^2 + dz^2) + \rho^2 d\tilde{\phi}^2] \\ &\quad - f(d\tilde{t} - \tilde{\omega}d\tilde{\phi})^2 \end{aligned} \quad (3)$$

$$\begin{aligned}(ds^2)_{CST} &= -e^{2\bar{\nu}}d\bar{t}^2 + B^2\sin^2\bar{\theta}(d\bar{\phi} - \bar{\omega}d\bar{t})^2 \\ &\quad + e^{2\alpha}(d\bar{r}^2 + \bar{r}^2 d\bar{\theta}^2) \end{aligned} \quad (4)$$

Ignoring terms of $\mathcal{O}(\epsilon^3)$, the HT metric components are

(cf. Abramowicz *et al.* 2003)[2]

$$
\begin{aligned}
g_{rr} &= \left(1-\frac{2M}{r}\right)^{-1}\left[1+j^2G_1+qF_2\right]+\mathcal{O}(\epsilon^3)\\
g_{tt} &= -\left(1-\frac{2M}{r}\right)\left[1+j^2F_1-qF_2\right]+\mathcal{O}(\epsilon^3)\\
g_{\theta\theta} &= r^2\left[1+j^2H_1-qH_2\right]+\mathcal{O}(\epsilon^3)\\
g_{\phi\phi} &= g_{\theta\theta}\sin^2\theta+\mathcal{O}(\epsilon^3)\\
g_{t\phi} &= \left(\frac{2jM^2}{r}\right)\sin^2\theta+\mathcal{O}(\epsilon^3)
\end{aligned}
$$

where

$$
\begin{aligned}
F_1 &= -pW+A_1,\\
F_2 &= 5r^3p(3u^2-1)(r-M)(2M^2+6Mr-3r^2)-A_1,\\
A_1 &= \frac{15r(r-2M)(1-3u^2)}{16M^2}\ln\left(\frac{r}{r-2M}\right),\\
A_2 &= \frac{15(r^2-2M^2)(3u^2-1)}{16M^2}\ln\left(\frac{r}{r-2M}\right),\\
G_1 &= p\left[(L-72M^5r)-3u^2(L-56M^5r)\right]-A_1,\\
H_1 &= A_2+(8Mr^4)^{-1}(1-3u^2)\times\\
&\times\ (16M^5+8M^4r-10M^2r^3+15Mr^4+15r^5),\\
H_2 &= -A_2+(8Mr)^{-1}5(1-3u^2)(2M^2-3Mr-3r^2),\\
L &= (80M^6+8M^4r^2+10M^3r^3+20M^2r^4-45Mr^5+15r^6),\\
p &= \left[8Mr^4(r-2M)\right]^{-1},\\
W &= (r-M)(16M^5+8M^4r-10M^2r^3-30Mr^4+15r^5)\\
&+\ u^2(48M^6-8M^5r-24M^4r^2-30M^3r^3\\
&-\ 60M^2r^4+135Mr^5-45r^6),
\end{aligned}
$$

with $u=\cos\theta$. The dimensionless angular momentum and quadrupole moment j and q are defined as:

$$j=J/M^2, \qquad q=Q/M^3. \tag{5}$$

The full Manko metric is rather lengthy and can be found in many papers (eg. Manko *et al.* 2000a, 2000b; Stute & Camenzind 2002; BS), so we will not give it explicitly here. We only recall that it depends on three parameters: the gravitational mass M, the angular momentum per unit mass $a=J/M$ and a third parameter b which is related to the quadrupole moment by

$$Q=-M(d-\delta-ab+a^2), \tag{6}$$

where

$$
\begin{aligned}
\delta &= \frac{-M^2b^2}{M^2-(a-b)^2},\\
d &= \frac{1}{4\left[M^2-(a-b)^2\right]}.
\end{aligned}
$$

The next non-zero multipole moment for the Manko metric is the current octupole, which is given by

$$S_3=-M\left[a^3-2a^2b+a[b^2+2(d-\delta)]-b(d-\delta)\right]. \tag{7}$$

[2] The original Hartle (1967) metric differs from the one presented here, in that it was not consistently truncated to order ϵ^2. The Abramowicz *et al.* (2003) preprint contains some minor sign errors.

For a detailed description of the CST metric we refer to the original paper (Cook *et al.* 1994). The extraction of multipole moments from the CST metric and the numerical calculation of ISCOs along evolutionary sequences are discussed in BS.

In vacuum, the HT metric is equivalent to the Kerr metric at second order in J when one sets $Q=J^2/M$, and reduces to the Schwarzschild solution when $J=Q=0$. It is not possible to obtain Kerr directly from the Manko metric by a smooth variation of the real parameters a, M and b. In other words, Kerr and Schwarzschild are not part of the 3 *real* parameter family of solutions described by the Manko metric. However they can be obtained by analytic continuation, setting $b^2=a^2-M^2$. Schwarzschild is a special case with $a=0$ and $b^2=-M^2$.

3 INTEGRATION OF THE HARTLE-THORNE EQUATIONS OF STRUCTURE

In this Section we outline some important aspects of the HT equations of structure. The relevant formalism was originally developed in (Hartle 1967), and the integration method is summarized in (Hartle & Thorne 1968). In the numerical code we used the reformulation of the equations of structure given in Appendix A of (Sumiyoshi *et al.* 1999). We refer to that paper for the equations [3].

As discussed in the Introduction, the HT metric is a slow rotation expansion in the angular velocity truncated to second-order. We consider the expansion parameter to be

$$\epsilon=\Omega/\Omega^* \ . \tag{8}$$

The solutions of the TOV equations for a given EOS form a one-parameter family, where, for example, one can use the star's central energy density ρ_c as the parameter. Similarly, solutions of the HT equations of structure form a two-parameter family. Natural parameters to label each model are the central energy density ρ_c and the rotational parameter ϵ.

Arriving at a particular HT model involves three conceptual stages. First, the stellar structure of a non-rotating star is obtained from the TOV equations, giving the non-rotating gravitational mass M and stellar radius R. Note that these non-rotating quantities are unlabelled. From these the rotational scale $\Omega^*=\sqrt{M/R^3}$ can be calculated. We can also compute the star's binding energy E_B, defined

[3] Comparing with the HT original papers, we found that Appendix A of (Sumiyoshi *et al.* 1999) contains a few typos:

- In Equation (A11), r^4 should be replaced with $r^2\xi$.
- In Equation (A14), R^4 should be replaced with r^4.
- In the last factor of Equation (A15), $r(r-2m)$ should be replaced with $(r-2m)$.
- In Equation (A36), p should be replaced with ρ_c.
- In Equation (A41), $e^{-\nu/2}$ should be replaced with $e^{\nu/2}$.
- In Equation (A54), ξ_0 should be replaced with ξ_2.

Notice also that Sumiyoshi *et al.* do not explicitly give boundary conditions at the center for the 'particular' solutions h_2^p, v_2^p. These boundary conditions are given in equations (128)-(130) of Hartle (1967); however, in equation (130) of Hartle's paper the factor 4π should be replaced by 2π.

as the difference between the baryonic mass M_b and the gravitational mass M:

$$E_B = M_b - M. \tag{9}$$

Second, a model with $\epsilon = 1$, i.e. a model rotating at the 'maximum' angular velocity of Ω^*, is obtained from the full HT equations. Here all quantities are labelled with a superscript asterisk : the model has gravitational mass $M^* = M + \delta M^*$, angular momentum J^*, and quadrupole moment Q^*. Finally, the model with the chosen value of $\epsilon < 1$ is calculated, having rotating gravitational mass $M^{(\epsilon)} = M + \delta M^{(\epsilon)}$, angular momentum $J^{(\epsilon)}$, and quadrupole moment $Q^{(\epsilon)}$.

The effects of rotation on the various quantities of interest appear at different orders in ϵ. The general relativistic frame dragging appears at first order, and the angular momentum is:

$$J^{(\epsilon)} = \epsilon J^*. \tag{10}$$

The radius of gyration R_g, defined so that the moment of inertia is $I = MR_g^2$, can then be calculated as

$$R_g = \left(\frac{I}{M}\right)^{1/2} = \left(\frac{J}{\Omega M}\right)^{1/2} = \left(\frac{J^*}{\Omega^* M}\right)^{1/2} + \mathcal{O}(\epsilon^2)\ , \tag{11}$$

where the first two relations are exact, and the third expresses the fact that computing R_g requires the integration of the equations of structure at first order in ϵ. However, involving the ratio of J and Ω (which are both proportional to ϵ) R_g does not depend on ϵ. For the same reason, computing the second order contribution to R_g would require third order corrections to J and Ω.

At second order in ϵ there appear corrections to the stellar eccentricity e_s, quadrupole moment Q, mass M, binding energy E_B, and coordinate stellar radius R. The stellar eccentricity is

$$e_s = \left[(R_e/R_p)^2 - 1\right]^{1/2}\ , \tag{12}$$

where R_e and R_p are the stellar coordinate radii at the equator and at the pole, respectively[4]. The quadrupole moment Q can be invariantly defined as the leading coefficient in the asymptotic behavior at large distances from the origin of the eccentricity of a family of spheroidal surfaces where the norm of the timelike Killing vector is constant. Taking into account that the zero order (non-rotating) values of e_s and Q are zero, we have

$$\begin{aligned} e_s^{(\epsilon)} &= \epsilon^2 e_s^*, \\ Q^{(\epsilon)} &= \epsilon^2 Q^*, \\ \delta M^{(\epsilon)} &= \epsilon^2 \delta M^*, \\ \delta E_B^{(\epsilon)} &= \epsilon^2 \delta E_B^*, \\ \delta R^{(\epsilon)} &= \epsilon^2 \delta R^*. \end{aligned} \tag{13}$$

This means, in particular, that for a fixed value of the central energy density, a stellar model rotating with angular velocity $\Omega = \epsilon\Omega^*$ has a gravitational mass

$$M^{(\epsilon)} = M + \epsilon^2 \delta M^*. \tag{14}$$

We have checked our numerical code by reproducing the results shown in Hartle & Friedman (1975) for polytropic EOSs. We found agreement on all significant digits for the quantities we have just defined. Then we chose the same set of 'realistic' EOSs used in BS, and verified that in the non-rotating limit our numerical results are consistent with Stergioulas' RNS code (described in Stergioulas & Friedman 1995).

For any given 'realistic' EOS, we can construct a sequence of rotating models by integrating the HT structure equations for a series of values of the central energy density. Our results are summarized in Tables 1-5. The chosen central energy density ρ_c, radius R, gravitational mass M, binding energy E_B and Ω^* are listed in the first five columns (marked by ϵ^0, since they do not depend on rotational corrections). At order ϵ we list the value of the radius of gyration R_g^* (from which the angular momentum J^* can be easily obtained) and of the frame dragging function ω_c^* at the center (normalized by Ω^*). Finally we list the second-order quantities $\delta R^*/R$, $\delta M^*/M$, $\delta E_B^*/E_B$, $Q^*/(MR^2)$ and e_s^*.

Let us stress again that although Ω^* is not the mass-shedding limit in a general relativistic framework, because of its physical meaning it does give an order of magnitude estimate of the mass shedding frequency, and so we can expect the HT treatment to break down when $\epsilon \sim 1$.

3.1 Matching the Hartle-Thorne and numerical spacetimes

To find a HT model that corresponds to a particular CST stellar model, say one belonging to the constant-rest mass sequences computed in BS using the RNS code, we adopt the following procedure, in which quantities obtained from the CST model are labeled with overbars : $\bar{M}$, $\bar{J}$ and $\bar{Q}$.

The aim is to find a HT model for which $M^{(\epsilon)} = \bar{M}$ and $J^{(\epsilon)} = \bar{J}$. Imposing these values on Eqs. (10) and (14) gives

$$\epsilon = \bar{J}/J^* \tag{15}$$

and

$$\bar{M} = M + (\bar{J}/J^*)^2 \delta M^*. \tag{16}$$

In (16), the quantities J^*, M and δM^* are effectively functions of ρ_c, since once ρ_c is specified they can be calculated from $\epsilon = 0$ or $\epsilon = 1$ models. Therefore, in order to find the matching HT model, we must search for a value of ρ_c for which Eq. (16) holds; ϵ is then given by Eq. (15).

In practice, we consider the function

$$f(\rho_c) = \bar{M} - \left[M + (\bar{J}/J^*)^2 \delta M^*\right]\ . \tag{17}$$

To locate the matching model with a given accuracy (that we set to 10^{-5}) we search for the root of Eq. (17) using bisection. Note that, since the HT expansion is a small-ϵ approximation, we expect to find solutions only for small values of the angular momentum $\bar{J}$. This turns out to be indeed the case.

In Table 6 we show some basic features of the matching

[4] In the notation of Hartle & Thorne (1968) the stellar radius $R(\theta) = R + \xi_0(R) + \xi_2(R)P_2(\cos\theta)$, where R is the non-rotating stellar radius, $\xi_0(r)$ and $\xi_2(r)$ are radial functions determined by the HT perturbation equations and $P_2(\cos\theta)$ is a Legendre polynomial. The equatorial radius $R_e = R(\pi/2)$, and the polar radius $R_p = R(0)$.

models for the five EOSs we consider. The HT models we compute are matched to the slowest-rotating models of the evolutionary sequences presented in Tables 1-5 of BS: as just mentioned, Eq. (17) has no solutions beyond some critical rotation rate.

For each EOS we present matching models for the 14 sequence above matching models for the MM sequence. From left to right we list: the central energy density $\bar{\rho}_c$ for which we find a matching solution (if such a central energy density exists); the value of $\epsilon = \bar{J}/J^*$ at the given central energy density; the gravitational mass $\bar{M}$ and the angular momentum $\bar{J}$, in geometrical units; the value of the quadrupole moment predicted by the HT equations of structure for the selected model, which scales as ϵ^2, and is given by

$$-M_2 = Q^{(\epsilon)} = (\bar{J}/J^*)^2 Q^*; \tag{18}$$

and finally,

$$\delta Q = 100(Q^{(\epsilon)} - \bar{Q})/\bar{Q}, \tag{19}$$

that is, the percentage deviation of the HT quadrupole moment from its value $\bar{Q}$ for the numerical spacetime, which can be found in Tables 1-5 of BS.

4 HOW ACCURATE IS THE SLOW-ROTATION EXPANSION?

In the previous Section we have seen how, given a numerical solution of the full Einstein equations with gravitational mass $M = \bar{M}$ and (small enough) angular momentum $J = \bar{J}$, we can construct a HT model matching the given values of M and J. Our purpose in this Section is to give two alternative, quantitative estimates of the difference between each of the HT matching models and the corresponding numerical model. The first estimate will be based on the calculation of the spacetimes' quadrupole moment as a function of the rotation rate; the second, on the calculation of the ISCO radii.

4.1 Deviations in the quadrupole moment

The matching models described in Section 3.1 are constructed by imposing that the first mass multipole M and the first current multipole J be the same as in the numerical spacetime. The HT solution is a two-parameter family: once ρ_c and ϵ are specified, the whole multipolar structure of the HT spacetime is. In particular, at second order in ϵ the HT structure equations predict a specific value for the quadrupole moment $Q^{\rm HT}$. Since multipole moments are global features of a spacetime (Fodor, Hoenselaers & Perjès 1989), we can measure the 'distance' of the HT spacetime from the numerical spacetime by looking at the difference between the value $Q^{\rm HT}$ predicted by the HT code, and the 'exact' value Q predicted by the RNS code. That is, we compute the relative deviation

$$\frac{\Delta Q}{Q} = \frac{Q^{HT} - Q}{Q}. \tag{20}$$

Given that the HT metric is exact in the limit $\epsilon \to 0$, but becomes less accurate for larger values of ϵ, we expect this deviation to increase with the rotation rate: an explicit calculation shows that this is indeed the case.

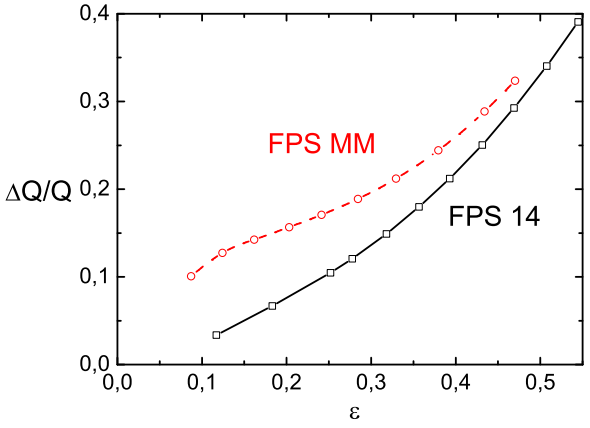

Figure 1. Relative error in the quadrupole moment for the FPS 14 sequence (squares) and the FPS MM sequence (circles).

As shown in Table 6, matching models – that is, solutions of Eq. (17) – only exist up to some critical value of the angular momentum J (and of the expansion parameter ϵ) where the HT approximation breaks down, and is unable to reproduce the numerical results. The deviation of $Q^{\rm HT}$ from the 'true' numerical value when $\epsilon \simeq 0.2$ depends slightly on the EOS, but it is typically $\sim 10\%$ for the 14 sequence and $\sim 20\%$ for the MM sequence. For the 14 sequence, the relative error becomes larger than 20 % when $\epsilon \sim 0.4$. From Table 6 one can see that deviations are not very sensitive to the EOS: for example, when $\epsilon \sim 0.4$ the relative error for the MM sequence ranges (roughly) between 25 % and 30 %. At fixed ϵ, $\Delta Q/Q$ is larger for the MM sequence than for the 14 sequence. However recall that Q is generally larger for low-mass evolutionary sequences, where gravity is weaker and centrifugal effects give the star a more oblate shape. Deviations in the ISCO radii, as given by Eq. (21) below, depend on the absolute value of Q. Since Q is larger for the 14 sequence, and percentage errors induced by the HT approximation are comparable to those for the MM sequence, the HT approximation should induce larger errors in the ISCO for the low-mass 14 sequence. This will be explicitly shown in Section 4.2.

Table 6 contains only a few slow-rotating models for each EOS. To get a better idea of what happens in the slow-rotation regime we have selected EOS FPS (which is quite average in terms of stiffness) and computed more numerical models for small values of J (that is, for small values of ϵ). Namely, we used the RNS code to compute 11 constant rest-mass models for the 14 sequence and 10 models for the MM sequence, spanning the range $\epsilon = 0$ to $\epsilon \sim 0.5$. To each of these models we matched a HT model. Results for the relative deviations in the quadrupole moment are shown in Fig. 1. The convergence to zero as $\epsilon \to 0$ is very smooth for the FPS 14 sequence. For the FPS MM sequence, the slowest rotating model seems to show a slight deviation from the general trend. We suspect this is due to a loss of accuracy of the RNS code in computing the comparatively smaller Q (for any given ϵ) of the more compact MM star models with small rotation rates. Indeed, when we compute

the curvature invariants for these models we also find some numerical noise: this can be seen by a close scrutiny of the bottom curve in the lower panels of Figs. 5, 6 and 7. The relative error $\Delta Q/Q$ is of the same order of magnitude in both cases, but it is systematically larger for the FPS MM sequence than for the FPS 14 sequence.

4.2 Deviations in Innermost Stable Circular Orbits

The exterior vacuum metric for a HT model truncated at second order in ϵ depends only on M, J and $Q = Q^{\rm HT}$. In particular, once we have computed these multipole moments we can use them to compute the coordinate ISCO radius using the results by Abramowicz *et al.* (2003). Using the dimensionless quantities j and q introduced in Eq. (5), their prediction for the *coordinate* ISCO radii is

$$r_\pm = 6M\left[1 \mp j\left(\frac{2}{3}\right)^{3/2} + j^2\left(\frac{251647}{2592} - 240\ln\frac{3}{2}\right) + q\left(-\frac{9325}{96} + 240\ln\frac{3}{2}\right)\right], \quad (21)$$

where r_+ refers to corotating orbits, and r_- to counterrotating orbits. The comparison of the HT ISCO radii as given by Eq. (21) to numerical results from the RNS code provides an alternative measure of the difference between a numerical model and the corresponding HT matching model.

We consider again the slow-rotating evolutionary sequence for EOS FPS described in Section 4.1. For each model along this evolutionary sequence we compute M, J and $Q^{\rm HT}$, and we plug those values in Eq. (21) to compute the *coordinate* ISCO radii. Then we can easily compute the *circumferential* ISCO radii for these equatorial orbits as

$$R_\pm^{\rm (HT)} = \sqrt{g_{\phi\phi}(r_\pm, \theta = \pi/2)}, \quad (22)$$

and compare our results with the numerical value of the circumferential ISCO radii[5] as obtained from RNS.

In Fig. 2 we show results for the FPS 14 sequence (top panel) and for the FPS MM sequence (bottom panel). In each panel we plot together, as functions of ϵ: 1) the circumferential radii R of the stars, 2) the corotating ISCOs R_+, 3) the counterrotating ISCOs R_-. Filled symbols are obtained from RNS, and empty symbols correspond to the HT matching models. The circumferential radius for each matching model is just

$$R_{e,\rm circ}^{\rm (HT)} = \sqrt{g_{\phi\phi}(R_e, \theta = \pi/2)}, \quad (23)$$

where R_e is the *coordinate* equatorial radius, obtained by integrating the HT equations of structure.

It is evident from Fig. 2 that for neutron stars of canonical mass $M \simeq 1.4 M_\odot$ the deviation of HT from the full numerical solution is larger. However, even in that case the HT approximation gives very accurate predictions both for the stellar equatorial radii and for the ISCO radii up to $\epsilon \simeq 0.3$. In particular, the fastest rotating model in the FPS 14 sequence for which a corotating ISCO exists has $\epsilon = 0.318$ and a spin frequency in physical units $\nu_{\rm phys} = \Omega_{\rm phys}/2\pi = 599$ s^{-1}, corresponding to an orbital period $P = 1.67$ ms. Therefore our calculation shows that the HT approximation accurately predicts ISCO radii down to periods which are comparable to that of the fastest observed millisecond pulsar, PSR J1939+2134, spinning at $P = 1.56$ ms (Backer *et al.* 1982).

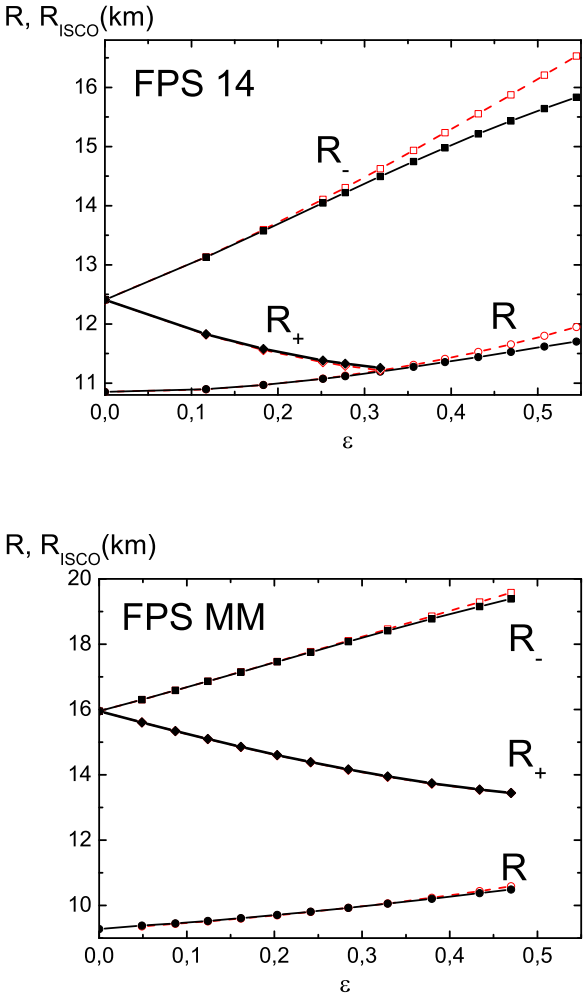

Figure 2. Filled circles give the stellar circumferential radius R, filled diamonds the circumferential radius of corotating ISCOs R_+ (when it exists) and filled squares the circumferential radius of counterrotating ISCOs R_- for the numerical spacetime. Empty symbols give the corresponding quantities for the HT metric. The top panel refers to the FPS 14 evolutionary sequence, the bottom panel to the FPS MM sequence.

Relative errors for corotating and counterrotating ISCOs are shown in Fig. 3 for both the FPS 14 and FPS MM sequences. In this plot we use the same convention as in BS: $\epsilon < 0$ corresponds to counterrotating orbits. As one would expect, errors tend to zero as $\epsilon \to 0$. The error for counterrotating ISCOs monotonically increases for large ϵ; the error for corotating ISCOs does not (at least for the FPS MM sequence) and it is typically extremely small (below 5 parts in a thousand, roughly the same accuracy as our numerical runs of the RNS code). We suspect that this could be

[5] These are given by $R_\pm = R_e + h_\pm$ in the notation of CST and BS.

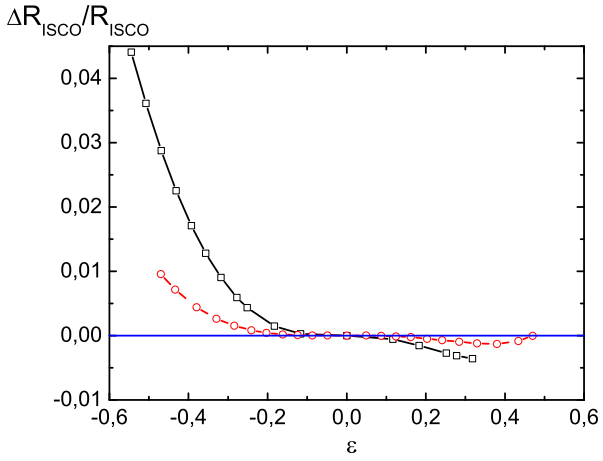

Figure 3. Relative error in the ISCO radii, $(R_+^{(HT)} - R_+)/R_+$ and $(R_-^{(HT)} - R_-)/R_-$, for the FPS 14 sequence (squares) and the FPS MM sequence (circles). In this plot we used the same convention as in BS: a negative ϵ (and a negative J) corresponds to counterrotating orbits.

due to the second order HT approximation being sufficiently accurate to compute the corotating ISCO, but not the counterrotating ones. To confirm our conjecture we would need to push the HT calculation to third order, which is beyond the scope of this paper.

As anticipated in Section 4.1, ISCO radii for the MM sequence agree better with the numerical results. Stars in the lower-mass FPS 14 evolutionary sequence have larger Q (they are more oblate), and relative errors in Q for both sequences are roughly comparable. Therefore effects due to the quadrupole moment on the location of the ISCO are larger for the lower-mass sequence. Notice also that, although deviations in the quadrupole moment can be as large as 20 % for stars rotating with $\epsilon \sim 0.3$, the relative errors on the ISCO are typically smaller than 1 % at the same rotation rates. This can be understood by looking at Eq. (21). For small rotation rates we have seen in Section 3 that $q = aj^2$, where a is a constant of order unity. This scaling property is actually more general, applying also to numerical solutions with large rotation rates: Laarakkers & Poisson (1999) showed that a depends on the EOS and on the mass of the stellar model, ranging between $a \simeq 2$ for high-mass models with soft EOSs and $a \simeq 12$ for low-mass models with stiff EOSs (cf. their Table 7; see also Miller 1977 for similar results in the HT approximation). The numerical coefficient of the j^2-dependent correction in Eq. (21) is $\simeq -0.226$, while the numerical coefficient of the q-dependent correction is $\simeq 0.176$: that is, the two coefficients are roughly equal in magnitude but opposite in sign. For this reason, shape-dependent effects in the ISCO (which are $\mathcal{O}(\epsilon^2)$) tend to cancel for small rotation rates. This explains why the HT approximation does such a good job in predicting the ISCO radii.

To better illustrate the physical significance of our results, in Fig. 4 we plot the relative errors in the quadrupole moments (top panel) and in the ISCO radii (bottom panel) as a function of the spin period P (in milliseconds) of our

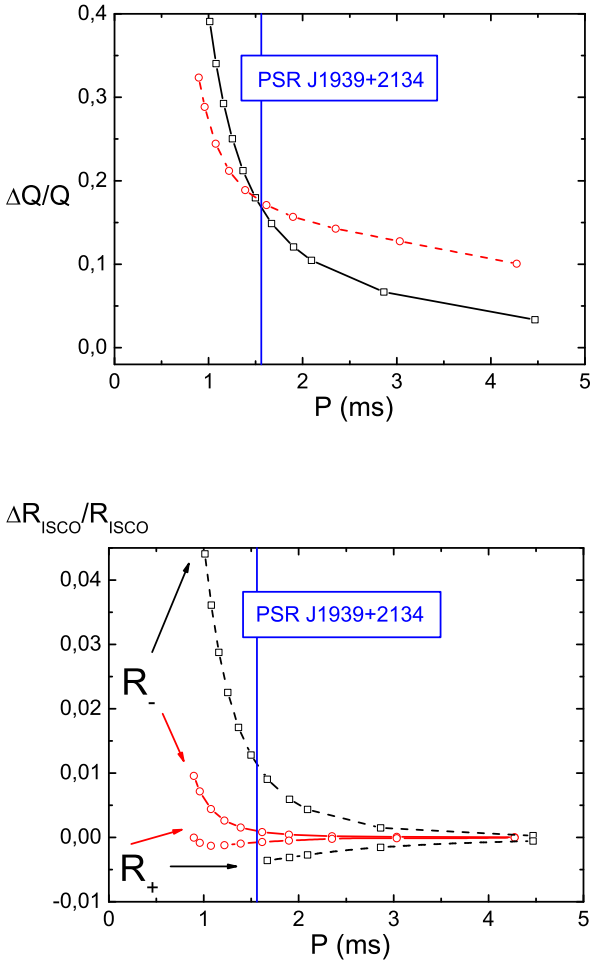

Figure 4. The top panel shows the relative error in the quadrupole moment for the FPS 14 sequence (squares) and the FPS MM sequence (circles) as a function of the spin period P of the star (in milliseconds). The bottom panel shows the relative error for corotating (R_+) and counterrotating (R_-) ISCO radii for the FPS 14 sequence (squares) and the FPS MM sequence (circles) as a function of P. In both panels, the vertical line marks the spin frequency of the fastest observed millisecond pulsar PSR J1939+2134.

rotating stellar models. This plot is useful for the following reasons. First of all, the relation between the HT expansion parameter ϵ and the rotational period of pulsars is non-linear. Not only is P proportional to $1/\epsilon$, it also has (for the constant-rest mass sequences we consider) a weak but non-trivial dependence on the parameters M and R:

$$P = \frac{2\pi}{\Omega} = \frac{2\pi}{\epsilon\Omega^*} = \frac{2\pi}{\epsilon(M/R^3)^{1/2}}\,. \tag{24}$$

Fig. 4 shows that all of our so-called 'slow rotation' models are actually millisecond pulsars, many of which rotate even faster than the fastest observed millisecond pulsar PSR J1939+2134 (Backer *et al.* 1982). This gives a concrete idea of the rotation rates we are considering in this paper.

In both panels we mark by a vertical line the spin frequency of PSR J1939+2134. The relative error in Q for a

pulsar spinning as fast as PSR J1939+2134 is of order 20 %, and this is quite independent of the stellar mass. Remarkably, the relative error in corotating and counterrotating ISCOs induced by the HT approximation is smaller than 1 %, even when the pulsar rotates with a period as small as 1.5 ms. This upper limit on deviations in the ISCO applies both to the FPS 14 sequence and to the FPS MM sequence.

For concreteness, in Fig. 4 we presented the specific example of PSR J1939+2134. However we wish to stress that our analysis can be considered more general. Even if faster pulsars were discovered, our conclusions are likely to be only marginally altered. Indeed, Chakrabarti *et al.* (2003) performed a statistical analysis of observations of 11 nuclear powered pulsars with spin frequencies between 270 Hz and 619 Hz. Their analysis implies an upper limit of 760 Hz (95% confidence level) on the spin frequency, to be compared with the 641 Hz of PSR J1939+2134. Therefore PSR J1939+2134 should be very close to the *maximum* spin frequency allowed for an isolated neutron star. Interestingly, the upper limit from burst oscillations is much lower than the mass-shedding limit predicted by most EOSs: some mechanism must be at work to halt pulsar spin-up while accretion is still active. A plausible explanation is gravitational wave emission, due either to the excitation of the r-mode instability or to the presence of an accretion-induced crustal quadrupole moment (see Chakrabarti *et al.* 2003 for a discussion).

5 WEYL SCALARS IN A QUASI-KINNERSLEY FRAME

In the remainder of this paper we concentrate on the vacuum surrounding our rotating stellar models. We compute the Weyl scalars for the HT, Manko and CST spacetimes and define the 'quasi-Kinnersley' frame (Section 5.1). In Section 5.2 we present the simple analytical results we obtained for the HT metric, and in Section 5.3 we describe the analogous calculation for the Manko and CST metrics. In Section 6 we give numerical results for all three spacetimes.

5.1 The quasi-Kinnersley tetrad

We introduce a Newman-Penrose null tetrad $\{l^a,\ n^a,\ m^a,\ \bar{m}^a\}$, where l^a and n^a are real and m^a and $\bar{m}^a$ are complex conjugate, satisfying the usual orthonormality conditions: $l^a n_a = 1$, $m^a \bar{m}_a = -1$, all other products zero. The Weyl scalars are the usual contractions of the Weyl tensor,

$$\begin{aligned}
\psi_0 &= -C_{pqrs} l^p m^q l^r m^s, \qquad (25)\\
\psi_1 &= -C_{pqrs} l^p n^q l^r m^s,\\
\psi_2 &= -C_{pqrs} l^p m^q \bar{m}^r n^s,\\
\psi_3 &= -C_{pqrs} l^p n^q \bar{m}^r n^s,\\
\psi_4 &= -C_{pqrs} n^p \bar{m}^q n^r \bar{m}^s.
\end{aligned}$$

The speciality index (Baker & Campanelli 2000) is defined as

$$S = 27 J^2 / I^3, \qquad (26)$$

where the curvature invariants I and J can be expressed as

$$\begin{aligned}
I &= 3(\psi_2)^2 - 4\psi_1\psi_3 + \psi_0\psi_4,\\
J &= -(\psi_2)^3 + \psi_0\psi_2\psi_4 + 2\psi_1\psi_2\psi_3 - \psi_4(\psi_1)^2 - \psi_0(\psi_3)^2.
\end{aligned}$$

We use the additional conventions that an NP tetrad with $\psi_1 = \psi_3 = 0$ is called transverse (Beetle & Burko 2002), and that if further $\psi_0 = \psi_4$ then it is called symmetric, in which case we may refer to $\psi_0 = \psi_4$ as ψ_{04}.

The interpretation of the Weyl scalars in the context of BH perturbation theory is that ψ_0 represents radiation along the l^a direction, ψ_4 represents radiation along the n^a direction, while ψ_2 describes the Coulomb effect due to the presence of a central mass and the frame dragging of the background Kerr spacetime. ψ_1 and ψ_3 are longitudinal effects of no physical interest that can be set to zero by the remaining tetrad freedom (Teukolsky 1973, Stewart & Walker 1974). In our case, however, and in general for a stationary spacetime of Petrov Type I, ψ_0 and ψ_4 represent transverse curvature deviations (cf. Szekeres 1965) from the Coulombian ψ_2 field due to rotation: see Eq. (40).

It is useful then to consider only transverse frames. In a Type D spacetime a frame can be found in which ψ_2 is the only non-zero scalar: we refer to this as the Kinnersley frame (cf. Teukolsky 1973). With an appropriate choice of parameters (see below) both the Manko and the HT metrics can be reduced to Type D spacetimes (i.e. Schwarschild and Kerr). Here we work in the symmetric tetrad which, under these parameter choices, becomes the Kinnersley frame. In this tetrad ψ_{04} is an effect due solely to the non-Type-D-ness of the full metrics. We call this tetrad the 'quasi-Kinnersley' tetrad (Nerozzi *et al.* 2004).

In a Type I spacetime, there are three distinct equivalence classes of transverse tetrads (Beetle & Burko 2002). Each class consists of all those transverse tetrads that can be related to each other by either the exchange freedom $l^a \leftrightarrow n^a$, or by a class III rotation[6]:

$$\begin{array}{lll}
l \to A^{-1} l & \psi_0 \to A^{-2} e^{2i\theta} \psi_0 & \psi_3 \to A e^{-i\theta} \psi_3\\
n \to A n & \psi_1 \to A^{-1} e^{i\theta} \psi_1 & \psi_4 \to A^2 e^{-2i\theta} \psi_4\\
m \to e^{i\theta} m & \psi_2 \to \psi_2 &
\end{array}$$

We find one particular transverse tetrad by making the ansatz that the real null vectors of the tetrad should be linear combinations of the Killing vectors ξ^a and φ^a

$$\begin{aligned}
l^a &= A\xi^a + B\varphi^a, \qquad (27)\\
n^a &= C\xi^a + E\varphi^a. \qquad (28)
\end{aligned}$$

We then impose the NP tetrad inner product conditions and make particular (arbitrary) choices of the remaining free parameters and signs (different choices may result in a different tetrad, but this would be related to the first by a class III rotation, and so would be in the same equivalence class). The result is

$$\begin{aligned}
l^a &= \frac{1}{\sqrt{2}} \frac{\sqrt{g_{33}}}{\sigma} \left[1, 0, 0, \frac{(-g_{03} - \sigma)}{g_{33}}\right], \qquad (29)\\
n^a &= \frac{1}{\sqrt{2}} \frac{\sqrt{g_{33}}}{\sigma} \left[1, 0, 0, \frac{(-g_{03} + \sigma)}{g_{33}}\right], \qquad (30)\\
m^a &= \frac{1}{\sqrt{2}} \left[0, \frac{i}{\sqrt{g_{11}}}, \frac{1}{\sqrt{g_{22}}}, 0\right], \qquad (31)
\end{aligned}$$

where

$$\sigma^2 = g_{03}^2 - g_{00} g_{33}. \qquad (32)$$

[6] The parameter θ used in this Section has obviously nothing to do with the angular coordinate in the HT metric.

To pick out a particular member of a class of tetrads one can choose the symmetric tetrad. This can always be found from a transverse tetrad through the following class III rotation

$$\hat{\psi}_2 = \psi_2, \qquad \hat{\psi}_{04} \equiv \hat{\psi}_0 = \hat{\psi}_4 = \sqrt{\psi_0 \psi_4}, \quad (33)$$

$$\Rightarrow \quad A^4 = |\psi_0|/|\psi_4| \quad , \qquad \theta = \frac{1}{4}\arctan\left[\frac{\Im\left(\overline{\psi}_0 \psi_4\right)}{\Re\left(\overline{\psi}_0 \psi_4\right)}\right], \quad (34)$$

where the $\hat{\psi}$'s are in the symmetric tetrad, the ψ's are in the non-symmetric tetrad and an overbar means complex conjugate. We do not write down the expressions for the tetrad vectors in the symmetric frame, since the parameters A and θ are very long if written out in full, making the expression unenlightening, but it is worth noting that since this is a class III rotation, the directions of the l^a and n^a vectors do not change.

We will call the above tetrad, built on the Killing vectors, T1. Using a method suggested by Burko (2003) we can show that if the non-zero scalars in the symmetric version of T1 are $\psi_{04}^{\rm T1}$ and $\psi_2^{\rm T1}$ then in the other two transverse *symmetric* tetrads (T2 and T3) the non-zero scalars are given by:

$$\textbf{T2} \qquad \psi_2^{\rm T2} = \frac{1}{2}\left(\psi_{04}^{\rm T1} - \psi_2^{\rm T1}\right) \quad (35)$$

$$\psi_{04}^{\rm T2} = \frac{1}{2}\left(\psi_{04}^{\rm T1} + 3\psi_2^{\rm T1}\right) \quad (36)$$

$$\textbf{T3} \qquad \psi_2^{\rm T3} = \frac{1}{2}\left(-\psi_{04}^{\rm T1} - \psi_2^{\rm T1}\right) \quad (37)$$

$$\psi_{04}^{\rm T3} = \frac{1}{2}\left(\psi_{04}^{\rm T1} - 3\psi_2^{\rm T1}\right) \quad (38)$$

Hence, once the scalars in one transverse tetrad are known, it is easy to calculate those in the other two frames. We have done this in the reductions of Manko and HT to the Type D metrics described in the next section. In each case it turns out that T3 is the Kinnersley tetrad, i.e. that frame in which, for the Type D metrics, ψ_2 is the only non-zero scalar. We therefore make all of the following analysis in T3. This means that we are making an analogous choice of tetrad in each metric, that all tetrad freedom is used up, and that ψ_{04} represents a pure Type I effect. Indeed, it is clear from the definition (33) that each of the ψ_{04}'s in each of the three transverse symmetric tetrads is the square root of one of the three corresponding curvature invariants ('radiation scalars') introduced by Beetle & Burko (2002)[7]. However, only ψ_{04} in the quasi-Kinnersley frame vanishes in the 'Type D limit', and therefore its value is an invariant measure of the deviation from Type D.

Finally, in any symmetric transverse frame (in particular, in the quasi-Kinnersley tetrad T3) Eq. (26) reduces to

$$S = 27\left[(-\psi_2^3 + \psi_2\psi_{04}^2)^2\right] / \left[(3\psi_2^2 + \psi_{04}^2)^3\right]. \quad (39)$$

S is equal to 1 in a Type D spacetime. $(1 - |S|)$ is also dimensionless; in this sense it is better than ψ_{04} as an invariant measure of the deviation from Type D. We will refer to $(1 - |S|)$ as the Non-Type-D-ness in the following.

[7] Although each of the three ψ_{04}'s is defined in a specific tetrad by Eq. (33), which is not *per-se* invariant under tetrad rotations of Type I and II, it can actually be expressed in terms of I and J only. See Beetle and Burko (2002) for more details.

5.2 The Hartle-Thorne Weyl scalars in the quasi-Kinnersley frame

The HT slow rotation parameter ϵ is *not* a perturbative parameter with respect to Type D: at linear order in ϵ the HT solution in vacuum is equivalent to the Kerr metric, which of course is Type D *at all orders* in ϵ. Discarding terms of $\mathcal{O}(\epsilon^3)$ and higher, the HT Weyl scalars in the quasi-Kinnersley (symmetric transverse, T3) tetrad have simple expressions:

$$\begin{aligned}(\psi_{04})_{HT} &= \frac{15\sin^2\theta}{32M^7r^3(r-2M)}(Q - Q_{\rm Kerr}) \times \\ &\times \left[3r^2(r-2M)^2\ln[r/(r-2M)]\right. \\ &+ \left. 2M(r-M)(2M^2+6rM-3r^2)\right], \end{aligned} \quad (40)$$

$$\begin{aligned}(\psi_2)_{HT} &= -\frac{M}{r^3} - \frac{3i\cos\theta J}{r^4} \\ &- \frac{1}{16M^6r^7}\left\{P_2(\cos\theta)\left[15r^7\ln\left(\frac{r}{r-2M}\right)\right.\right. \\ &- 10Mr^2(8M^4+6M^3r+4M^2r^2+3Mr^3+3r^4) \\ &- \left.\left. 16M^6(r-6M)\right] - 16M^5r(r-M)\right\}J^2 \\ &+ \frac{1}{16M^5r^4}P_2(\cos\theta)\left[15r^4\ln\left(\frac{r}{r-2M}\right)\right. \\ &- \left. 10M(3r^3+4rM^2+3r^2M+6M^3)\right]Q. \end{aligned} \quad (41)$$

For a Kerr BH $Q = Q_{\rm Kerr} = J^2/M$, and it is immediately seen that $\psi_{04} = 0$ (as it should). Writing the above relations as Taylor series of the form

$$\begin{aligned}\psi_2 &= \psi_2^{(0)} + \psi_2^{(1)}\epsilon + \psi_2^{(2)}\epsilon^2 + \mathcal{O}(\epsilon^3), \\ \psi_{04} &= \psi_{04}^{(2)}\epsilon^2 + \mathcal{O}(\epsilon^3), \end{aligned} \quad (42)$$

it is easy to show that

$$1 - S = 3\left(\frac{\psi_{04}^{(2)}}{\psi_2^{(0)}}\right)^2\epsilon^4 + \mathcal{O}(\epsilon^5) = 3\left(\frac{\psi_{04}}{\psi_2}\right)^2 + \mathcal{O}(\epsilon^5). \quad (43)$$

Remarkably, the leading-order correction of S around its Type D value $S = 1$ is only of order ϵ^4: a fact due to S being a non-linear function of the Weyl scalars. Indeed, this doesn't mean that perturbations of order ϵ^2 do not alter the speciality condition: rather, $(1-S)$ is quadratic in these perturbations[8]. This is quite a subtle point, that can better be understood by explicitly constructing the principal null directions. Such a construction has been worked out in detail by Cherubini *et al.* (2004) for the simpler case of the vacuum Kasner spacetimes: cf. in particular the discussion following their Eq. (2.15). Furthermore, at leading order in the expansion the Non-Type-D indicators $1 - S$ and ψ_{04}/ψ_2 are completely equivalent to each other. In Section 6 we show by explicit calculations that this equivalence of the two Type D indicators is in fact more general: it holds true (at least approximately) for fully relativistic rotating star spacetimes as well. From Eq. (40) we also see that $(\psi_{04})_{HT}$ is proportional to $(Q - Q_{\rm Kerr})$. In other words, at leading order deviations from Type D are driven by the deviation of the quadrupole

[8] It is easy to check, using an expansion like (42) extended to higher order, that the leading fourth-order term in (43) will not change.

moment from its Kerr value, as we would expect on physical grounds.

From Eqs. (40) and (41) the asymptotic behavior of the Weyl scalars for large r at leading order is:

$$(\psi_{04})_{HT} \sim \frac{3\sin^2\theta(Q-Q_{\rm Kerr})}{2r^5}\,, \quad (44)$$

$$(\psi_2)_{HT} \sim -\frac{M}{r^3}\,. \quad (45)$$

Consequently, for the variables we use to measure deviations from Type D, at large r we have:

$$\left|\frac{\psi_{04}}{\psi_2}\right| \sim \frac{3\sin^2(\theta)}{2Mr^2}(Q-Q_{\rm Kerr})\,, \quad (46)$$

$$1-S \sim \frac{27\sin^4(\theta)}{4M^2r^4}(Q-Q_{\rm Kerr})^2\,. \quad (47)$$

Finally, as a useful check of our results, we show that ψ_2 reduces to the correct limit in the Kerr case. The proof is quite straightforward. To avoid confusion, let us denote the standard Boyer-Lindquist coordinates for the Kerr metric as (s,α) instead of (r,θ). Then the only non-zero Weyl scalar for the Kerr metric in the Kinnersley frame is given by

$$(\psi_2)_{\rm Kerr} = \frac{-M}{(s-ia\cos\alpha)^3}. \quad (48)$$

The relation between the two sets of coordinates is[9]:

$$s = r\left\{1-\frac{a^2}{2r^2}\left[\left(1+\frac{2M}{r}\right)\left(1-\frac{M}{r}\right)\right.\right. \quad (49)$$
$$\left.\left. - \cos^2\theta\left(1-\frac{2M}{r}\right)\left(1+\frac{3M}{r}\right)\right]\right\},$$

$$\alpha = \theta - a^2\cos\theta\sin\theta\frac{1}{2r^2}\left(1+\frac{2M}{r}\right). \quad (50)$$

Carrying out these coordinate transformations on equation (48), setting $J=Ma$, $Q=J^2/M$, and discarding terms of $\mathcal{O}(J^3)$, we get

$$(\psi_2)_{\rm Kerr} = -\frac{M}{r^3} - \frac{3i\cos\theta J}{r^4} \quad (51)$$
$$+ \frac{3}{2}\frac{(r-M)}{r^7M}\left[(6M+5r)\cos^2\theta-(2M+r)\right]J^2$$

This same expression is obtained from equation (41) when $Q=J^2/M$ is substituted.

This confirms that in T3, with the parameters set for Kerr, we indeed have the Kinnersley frame, and that with these parameters, ψ_2 is the only non-zero Weyl scalar and matches the analytically known expression. Clearly the further reduction to Schwarzschild ($J=Q=0$) also gives the correct known expression for $(\psi_2)_{\rm Schw}$.

5.3 The Manko and CST Weyl scalars in the quasi-Kinnersley frame

For the Manko metric we computed the Weyl scalars in the quasi-Kinnersley frame by the procedure described in Section 5.1, using the algebraic manipulation program *Maple*. However the final analytic expressions are very long and unenlightening, so we do not give them here. As a check, we verified numerically that in the quasi-Kinnersley frame $(\psi_{04})_{Manko}$ is zero when the Manko parameters are set to Kerr ($b^2=a^2-M^2$) or Schwarzschild ($a=0$, $b^2=-M^2$).

For the CST metric we followed again the same procedure, but in this case we had to solve a numerical problem. The Weyl scalars depend on first and second order partial derivatives of the metric coefficients. For the analytical spacetimes (HT and Manko) the computation of the scalars is a trivial process. However, for the numerical spacetime one has to invoke numerical differentiation. The second order radial derivatives turn out to be more sensitive to numerical error. Therefore we find that it is advantageous to avoid using second order radial derivatives calculated straight from a second order finite difference scheme. Instead we use the Ricci identities in the Newman-Penrose formalism. These allow us to express all second order radial derivatives in terms of second order angular derivatives and first order derivatives. Once we do this, the numerical calculation of the Weyl scalars turns out to be second order convergent on our numerical grid.

6 NON-TYPE-D-NESS OF THE EXTERIOR VACUUM

Using the procedure described in the previous Section we can compute the non-zero Weyl scalars ψ_2 and ψ_{04} in the quasi-Kinnersley frame for all three metrics (HT, Manko and CST). Then we can evaluate the Non-Type-D-ness $(1-|S|)$ and the ratio $|\psi_{04}/\psi_2|$. To avoid unnecessary complications, in the following we will restrict consideration to the equatorial plane.

In Fig. 5 we plot the invariant Non-Type-D-ness $(1-|S|)$ as a function of the circumferential radius $R_{\rm circ}$ for the CST metric. Throughout this section we will always refer to circumferential radii, which are operationally well-defined quantities (whatever approximation we use for the metric in the stellar exterior). For example, for a HT model the circumferential stellar radius on the equator is simply $\left[g^{\rm (HT)}_{\phi\phi}(R_e,\theta=\pi/2)\right]^{1/2}$, where R_e is the coordinate radius. The stellar radius in Manko coordinates ρ_e can be evaluated using the procedure described in Section 4.1 of BS. Once again, it's a simple matter to compute the corresponding equatorial circumferential radius $\left[g^{\rm (Manko)}_{\phi\phi}(\rho_e,z=0)\right]^{1/2}$ for the Manko models. Of course the fact that we are using different approximations for the metric will induce deviations between these stellar radii, but those deviations are typically below 1 % or so, even for the fastest rotating models.

In both panels of Fig. 5, lines from bottom to top give $(1-|S|)$ as a function of the circumferential radius $R_{\rm circ}$ for different values of the rotation rate. Since the calculation only applies to the vacuum exterior spacetime, each line starts from the star's circumferential equatorial radius ($R_{\rm circ}\geq R_e$). The plot shows that $(1-|S|)$ has the essential properties required of a Non-Type-D-ness: first of all, slower rotating model are supposed to be closer to Type D, and indeed $(1-|S|)$ is smaller; secondly, as $R_{\rm circ}\to\infty$ the spacetime becomes asymptotically flat and $(1-|S|)$ tends to zero.

[9] For the HT metric to reduce to the Kerr metric we must set $J=Ma$, $Q=J^2/M$ and ignore terms of $\mathcal{O}(J^3)$. Formula (A5) in (Hartle & Thorne 1968) contains a typo: in the r transformation, $\cos^2\theta$ should be replaced by $-\cos^2\theta$.

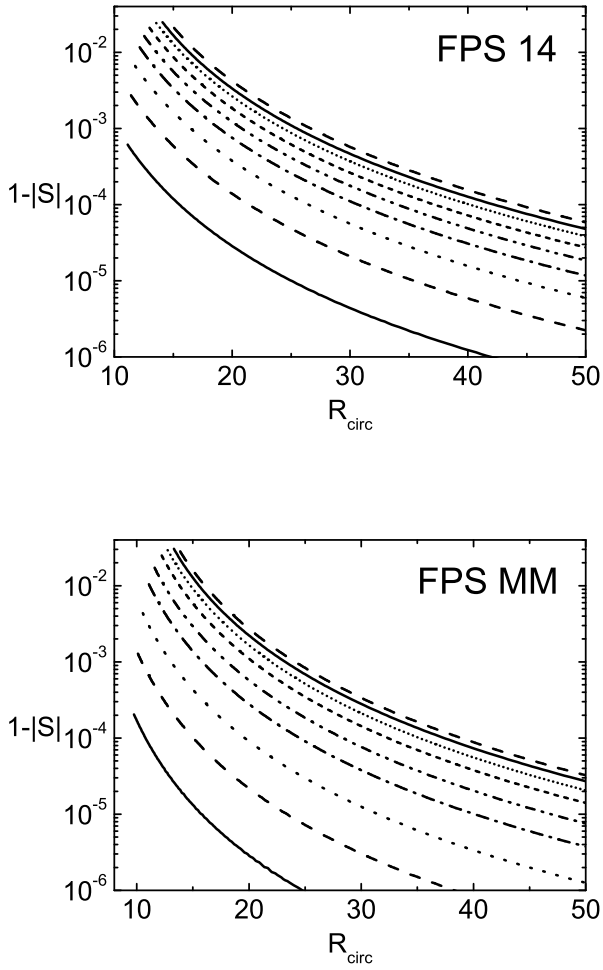

Figure 5. Non-Type-D-ness $(1-|S|)$ for the FPS 14 (top panel) and FPS MM (bottom panel) sequences, computed using the CST metric, as a function of the circumferential radius $R_{\rm circ}$. Within each panel, lines from bottom to top give $(1-|S|)$ as a function of the circumferential radius for different values of the rotation rate: slower rotating models are closer to Type D, so $(1-|S|)$ is smaller. Since the calculation only applies to the vacuum exterior spacetime, each line starts from the star's circumferential equatorial radius R_e.

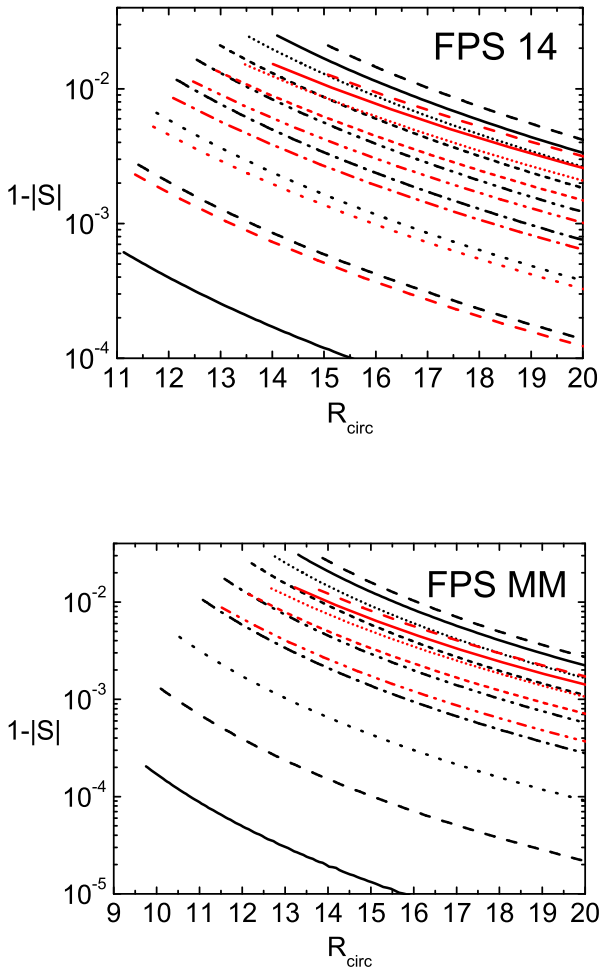

Figure 6. Close-up view of Fig. 5. Once again, the top panel refers to the FPS 14 sequence and the bottom panel to the FPS MM sequence. In red we overplot the Non-Type-D-ness for the Manko matching models, to visualize the difference with respect to the corresponding CST models.

For slowly rotating models (roughly speaking, for $\epsilon < 0.4$), the lower lines in Fig. 5 show that deviations from speciality are at most of order 1 %. So in most astrophysical situations it may make sense to use a Type D approximation: that is, to consider the exterior spacetime of a rotating star as a Kerr background, small corrections being induced by the star's oblate structure. This Type D approximation might be particularly useful for imposing boundary conditions in the computation of gravitational waves from rotating relativistic stars. Indeed, the gravitational wave amplitude dies out only as $1/r$, while our analysis shows that effects due to deviations from Type D die out faster than $1/r$. Therefore, far enough from the star the gravitational wave amplitude should (in some sense) be large enough that we can ignore the error made by using the Kerr approximation. On the other hand, the Kerr metric usually has a quadrupole moment that is 2 to 12 times smaller than that of a rapidly rotating star (Laarakkers & Poisson 1999). So, as long as we are in a regime in which the quadrupole moment affects the gravitational wave emission, the contribution of the quadrupole term will be underestimed by the corresponding factor. Only when we are far enough away that only the first-order terms in ϵ matter do the neutron star and BH spacetimes agree. In this sense Kerr is not a good replacement for HT to order ϵ^2, because of the large difference in the quadrupole moment. Using HT to order ϵ^2 should give a much more accurate waveform consistent to this order. A wave extraction formalism which is consistent to second order in ϵ is therefore worth developing.

Fig. 6 shows a close-up view of the strong field region of Fig. 5. In red we overplot the Non-Type-D-ness we computed for the matching Manko models (when they exist: recall that the Manko solution can only be matched to fast

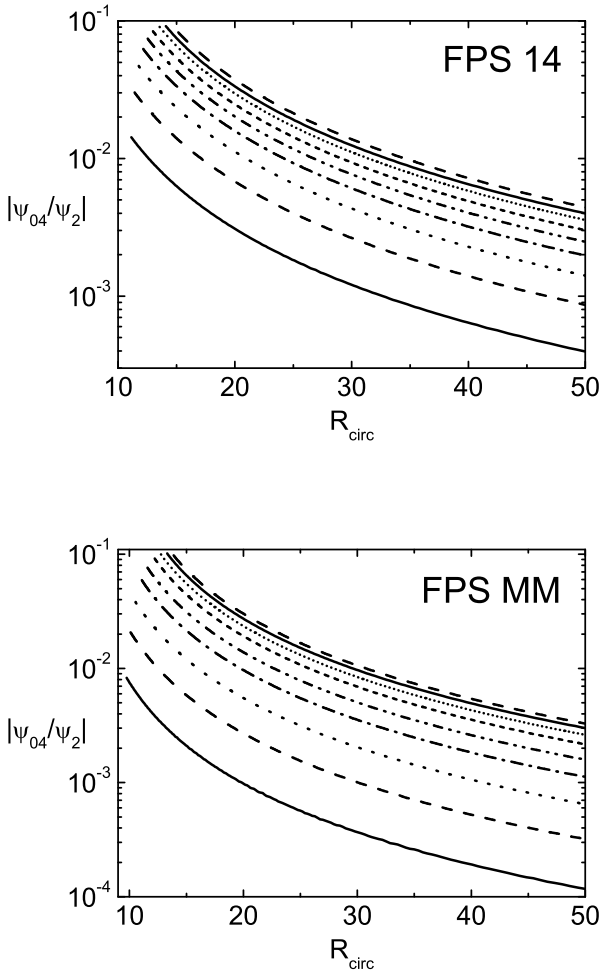

Figure 7. Ratio $|\psi_{04}/\psi_2|$ for the FPS 14 (top panel) and FPS MM (bottom panel) sequences, computed using the CST metric, as a function of the circumferential radius $R_{\rm circ}$. See the caption of Fig. 5 for more details.

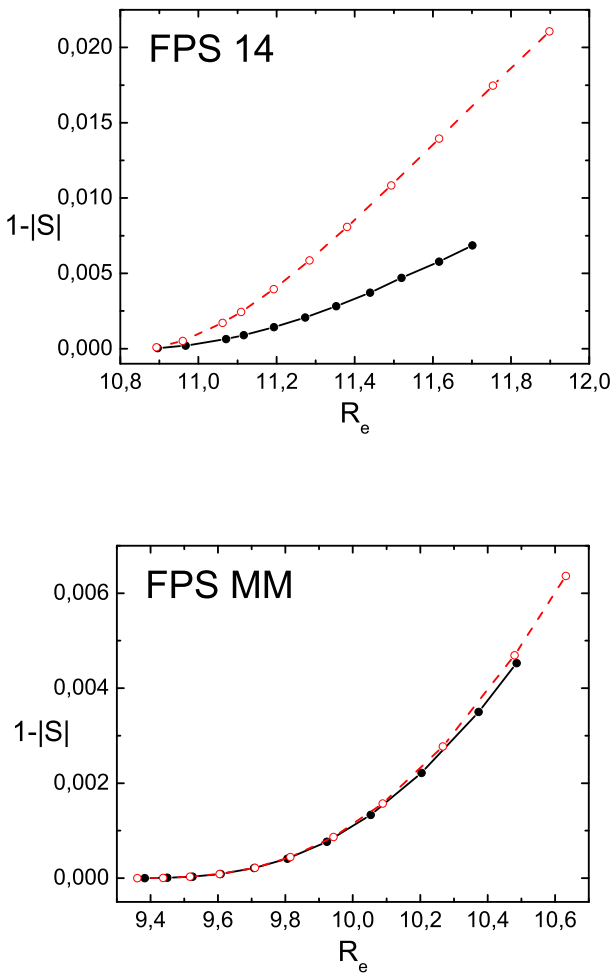

Figure 8. Non-Type-D-ness evaluated at the star's circumferential equatorial radius R_e, as a function of R_e, for the FPS 14 and FPS MM sequences (top and bottom panel, respectively). Filled circles correspond to CST models, empty circles correspond to matched HT models.

rotating models). For both sequences and for all values of the rotation rate the Manko metric is closer to Type D than the corresponding numerical model.

In Fig. 7 we plot the ratio $|\psi_{04}/\psi_2|$ as a function of the circumferential radius $R_{\rm circ}$ for the CST metric. As expected from our discussion in Sec. 5.1, the qualitative behavior is the same as in Fig. 5. $|\psi_{04}/\psi_2|$ is not invariant (ψ_{04} is a curvature invariant, in the sense discussed above, but ψ_2 is not), but it has the advantage of being dimensionless. One may want to develop a 'quasi-Type-D' approximation for perturbations of rotating NSs in the framework of the NP formalism, similar to the Teukolsky formalism for BHs. In this context the perturbed ψ_0 and ψ_4 would represent radiation, typically decaying as $1/r$. Then the value of the background ψ_{04} would be a useful number to consider for comparison. It is clear from Eq. (44) for the HT approximation and from Fig. 7 for the CST metric that ψ_{04} decays faster than $1/r$.

One might think that the value of the Non-Type-D-ness at the equatorial stellar radius, which is a physically well-identified location, could give an invariant measure of the deviation from speciality of each rotating stellar model. This is indeed the case for slowly rotating stars. In Fig. 8 we plot the value of $(1-|S|)$ at the equatorial circumferential stellar radius R_e as a function of R_e for our slowly rotating FPS 14 and FPS MM sequences. This quantity has the behavior expected of a Non-Type-D-ness in this rotational range: both for the CST metric and for the HT metric it increases with R_e (and with the rotation rate). Furthermore, it is larger for the FPS 14 sequence than for the FPS MM sequence. Once again, this is reasonable: low-mass models are more oblate than high-mass models, and their exterior spacetime is expected to deviate more from that of a BH.

From Fig. 5 and Fig. 6 it is clear that, at a given circumferential radius, $(1-|S|)$ increases with the stellar rotation rate. However, for large rotation rates $(1-|S|)$ *at the stellar equator* does *not* increase monotonically with rotation: we show this peculiar effect in Fig. 9. In other words, this sin-

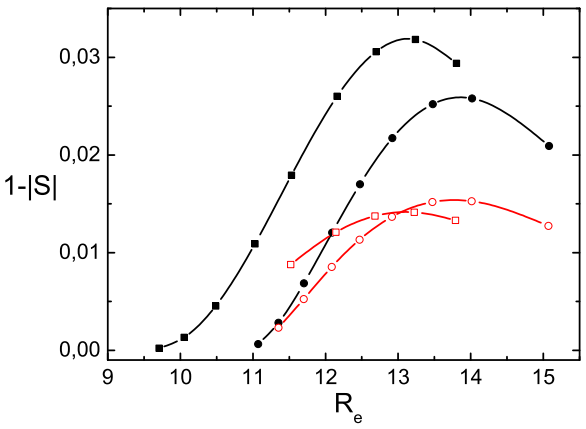

Figure 9. Non-Type-D-ness evaluated at the star's circumferential equatorial radius R_e, as a function of R_e, for the two sequences FPS 14 (circles) and FPS MM (squares). Filled symbols correspond to CST models, empty symbols correspond to matching Manko models (when they exist: cfr. BS).

gle number cannot be used to measure the deviation from speciality of a very fast rotating stellar model. To understand the reason for this non-monotonic behavior we can look again at Fig. 6. At any given circumferential radius $R_{\rm circ}$, $(1-|S|)$ does increase as the star spins faster. However the stellar circumferential radius (the value of $R_{\rm circ}$ at which each line starts) increases as well, due to the centrifugal deformation of the star. The two effects compensate, so that $(1-|S|)$ at the stellar radius shows a *maximum* as a function of the rotation rate. From Fig. 9 we see that this maximum shows up at the same rotation rate both for the CST metric and for the Manko matching models.

7 CONCLUSIONS

In this paper we compared three different approaches to the computation of rotating relativistic star spacetimes: the HT slow-rotation approximation, the Manko analytic vacuum solution, and numerical solutions of the full Einstein equations obtained using the CST self-consistent field method. We first integrated the HT structure equations for five representative equations of state, keeping terms up to second order in the slow-rotation parameter ϵ. Then we matched these models to the CST solutions, imposing that the gravitational mass and angular momentum of the models be the same. We estimated the limits of validity of the slow-rotation expansion computing deviations in the spacetime's quadrupole moments and in the ISCO radii at different rotation rates. We found that deviations in the quadrupole moment are $\sim$ 20 % for pulsars spinning with a period $\simeq 1.5$ milliseconds (the spin period of the fastest known pulsar, PSR J1939+2134). However, for these same spin rates deviations in the ISCO radii are always smaller than ~ 1 %. Since the HT approximation gives excellent predictions for ISCOs up to the fastest pulsar spin periods, it can safely be used whenever a full numerical solution would be too cumbersome to implement.

In the second part of the paper we focused on the exterior vacuum spacetime. We compared the HT approximation and the Manko analytic solution with numerical models using coordinate-independent quantities. For all three spacetimes we first introduced symmetric transverse frames, in which the only non-zero Weyl scalars are ψ_2 and $\psi_0 = \psi_4 \equiv \psi_{04}$. From those frames we then selected what we call the 'quasi-Kinnersley' frame (cf. Nerozzi *et al.* 2004): the frame in which ψ_2 is the *only* non-zero scalar when we set the parameters to reduce the metric to Type D. We computed ψ_2 and ψ_{04} in this frame. The latter is a scalar curvature invariant (Beetle & Burko 2002) that vanishes for Type D, and therefore its value is a measure of what one would call 'Non-Type-D-ness'. For the HT metric the use of the quasi-Kinnersley frame led us to very simple analytic expressions for ψ_2 and ψ_{04}. Due to their simplicity, our Eqs. (40) and (41) may be useful in different contexts. Furthermore, from Eq. (40) we reached the important conclusion that, at leading order, the deviation from Type D is linear in the deviation of the quadrupole moment from its Kerr value, $(Q-Q_{\rm Kerr})$. Therefore neutron stars with smaller mass and stiffer EOS deviate more from Type D.

Finally we evaluated the (scalar curvature invariant) speciality index S introduced by Baker & Campanelli (2000). Being dimensionless, $(1-|S|)$ is a better indicator of 'Non-Type-D-ness'. As ψ_{04}, it increases with rotation rate and goes to zero at infinity for any given rotation rate. At leading order from Eq. (43) $(1-S) \propto (\psi_{04}/\psi_2)^2$. However, it is not easy to give a single number characterizing the Non-Type-D-ness of a given spacetime. One might think about using the value of $(1-|S|)$ *at the stellar radius* for this purpose. This idea does not work in practice: since stellar models become more and more oblate as rotation increases, $(1-|S|)$ at the stellar radius eventually shows a *maximum* as a function of the rotation rate.

Although deviations from Type D increase for fast rotation, our results show that they can be expected to be rather small (less than a few percent) for astrophysically relevant rotation rates. This suggests that, in perturbative calculations of gravitational wave emission, rotating star exteriors can reasonably be approximated as Kerr-like spacetimes, or that one could develop an appropriate quasi-Type D approximation. The tools we have illustrated here will help to quantify the accuracy of such approximations, and hence to estimate numerical errors involved in the calculations of gravitational waves from rotating relativistic stars.

Acknowledgements

We would like to thank Lior Burko for very kindly providing us with notes on the method to identify the three transverse frames, and the anonymous referee for insightful comments. We also thank Marek Abramowicz, Joachim Almergren, Nils Andersson, Christian Cherubini, Wlodek Kluźniak, Kostas Kokkotas, John Miller, Andrea Nerozzi, Luciano Rezzolla, Adam Stavridis, Nick Stergioulas, Arun Thampan and Clifford Will for useful discussions. This work has been partly supported by the EU Programme 'Improving the Human Research Potential and the Socio-Economic Knowledge Base' (Research Training Network

Contract HPRN-CT-2000-00137). FW is supported by a EPSRC studentship.

REFERENCES

M. Abramowicz, G. J. E. Almergren, W. Kluźniak, A. V. Thampan, 2003, gr-qc/0312070.
N. Andersson, K. D. Kokkotas, 2001, Int. J. Mod. Phys. D 10, 381.
M. Ansorg, A. Kleinwaechter, R. Meinel, 2002, Astron. Astrophys. 381, L49.
D. C. Backer, S. R. Kulkarni, C. Heiles, M. M. Davis, W. M. Goss, 1982, Nature 300, 615.
J. Baker, M. Campanelli, 2000, Phys. Rev. D, 62, 127501.
C. Beetle, L. M. Burko, 2002, Phys. Rev. Lett. 89, 271101.
E. Berti, N. Stergioulas, 2004, MNRAS 350, 1416.
M. Bocquet, S. Bonazzola, E. Gourgoulhon, J. Novak, 1995, Astron. Astrophys. 301, 757.
S. Bonazzola, E. Gourgoulhon, M. Salgado, J.-A. Marck, 1993, Astron. Astrophys. 278, 421.
S. Bonazzola, E. Gourgoulhon, J.-A. Marck, 1998, Phys. Rev. D 58, 104020.
L. Burko, private communication, 2003.
D. Chakrabarty, E. H. Morgan, M. P. Muno, D. K. Galloway, R. Wijnands, M. van der Klis, C. B. Markwardt, 2003, Nature 424, 42.
S. Chandrasekhar, 1983, The Mathematical Theory of Black Holes, Oxford University Press.
S. Chandrasekhar, J. C. Miller, 1974, MNRAS 167, 63.
C. Cherubini, D. Bini, M. Bruni and Z. Perjes, 2004, Class. Quant. Grav. 21, 4833.
N. A. Collins, S. A. Hughes, 2004, Phys. Rev. D 69, 124022.
G. B. Cook, S. L. Shapiro, S. A. Teukolsky, 1994, Ap. J., 424, 823.
J. L. Friedman, J. R. Ipser, L. Parker, 1986, Ap. J. 304, 115.
G. Fodor, Z. Perjès, 2000, Gen. Rel. Grav. 32, 2319-2332.
G. Fodor, C. Hoenselaers, Z. Perjès, 1989, J. Math. Phys. 30, 2252.
J. B. Hartle, 1967, Ap. J., 150, 1005.
J. B. Hartle, J. L. Friedman, 1975, Ap. J. 196, 653.
J. B. Hartle, K. S. Thorne, 1968, Ap. J., 153, 807.
K. D. Kokkotas, J. Ruoff, 2002, in *Florence 2001, A relativistic spacetime odyssey*, 325; see also gr-qc/0212105.
H. Komatsu, Y. Eriguchi, I. Hachisu, 1989, MNRAS, 237, 355.
S. R. Kulkarni, 1995, in *Millisecond Pulsars. A Decade of Surprise*, volume 72 of *ASP Conference Series*, 79.
W. G. Laarakkers, E. Poisson, 1999, Ap. J., 512, 282.
V. S. Manko, E. W. Mielke, J. D. Sanabria-Gómez, 2000a, Phys. Rev. D 61, 081501(R).
V. S. Manko, J. D. Sanabria-Gómez, O. V. Manko, 2000b, Phys. Rev. D 62, 044048.
A. Nerozzi, C. Beetle, M. Bruni, L. M. Burko, D. Pollney, gr-qc/0407013.
J. C. Miller, 1977, MNRAS 179, 483.
T. Nozawa, N. Stergioulas, E. Gourgoulhon, Y. Eriguchi, 1998, Astron. Astrophys. Suppl. Ser. 132, 431.
D. Pollney, J. E. F. Skea, R. A. d'Inverno, 2000, Class. Quant. Grav. 17, 643.
V. Re, M. Bruni, D. R. Matravers, F. T. White, 2003, Gen. Rel. Grav. 35, 1351.
L. Rezzolla L., F. K. Lamb, S. L. Shapiro, 2000, Ap. J. 531, L141.
F. D. Ryan, 1995, Phys. Rev. D 52, 5707.
F. D. Ryan, 1997, Phys. Rev. D 55, 6081.
M. Salgado, S. Bonazzola, E. Gourgoulhon, P. Haensel, 1994, Astron. Astrophys. 291, 155.
M. Shibata, M. Sasaki, 1998, Phys. Rev. D 58, 104011.
N. R. Sibgatullin, 1991, Oscillations and waves in strong gravitational and electromagnetic fields (Engl. transl.), Springer, Berlin [orig. Russian, 1984, Nauka, Moscow].
H. C. Spruit, 1999, Astron. Astrophys. 341, L1.
H. Stephani, 2004, Relativity: An Introduction to Special and General Relativity, Cambridge University Press.
H. Stephani ,D. Kramer, M. MacCallum ,C. Hoenselaers ,E. Herlt, 2003, Exact Solutions of Einstein's Field Equations, Cambridge University Press.
N. Stergioulas, 2003, *Rotating Stars in Relativity*, Living Reviews in Relativity.
N. Stergioulas, J. L. Friedman, 1995, Astrophys. J. 444, 306.
J. M. Stewart, M. Walker, 1974, Proc. R. Soc. Lond. A 341, 49.
M. Stute, M. Camenzind, 2002, MNRAS 336, 831.
K. Sumiyoshi, J. Ma. Ibàñez, J. V. Romero, 1999, Astron. Astrophys. Suppl. Ser. 134, 39.
S. Szekeres, 1965, J. Math. Phys. 6, 1387.
S. A. Teukolsky, 1973, Ap. J. 185, 635.
F. Weber, N. K. Glendenning, 1992, Ap. J. 390, 541.

Table 1. Results of the HT integrations for EOS A. From left to right we list: the central energy density ρ_c; the stellar radius R, gravitational mass M and binding energy E_B for the non-rotating configuration; $\Omega^* = (M/R^3)^{1/2}$. Then we give quantities of order ϵ in rotation: the radius of gyration R_g^* and the frame dragging function ω_c^* at the center (normalized by Ω^*). In the last five columns we give quantities of order ϵ^2, namely the rotational corrections on radius ($\delta R^*/R$), mass ($\delta M^*/M$) and binding energy ($\delta E_B^*/E_B$), the quadrupole moment $Q^*/(MR^2)$ and the eccentricity e_s^*. Units are given where appropriate.

	$\sim\epsilon^0$				$\sim\epsilon$		$\sim\epsilon^2$				
ρ_c (g cm^{-3})	R (km)	$M/M_\odot$	$E_B/M_\odot$	Ω^* (km^{-1})	R_g^*/R	ω_c^*/Ω^*	$\delta R^*/R$	$\delta M^*/M$	$\delta E_B^*/E_B$	$Q^*/(MR^2)$	e_s^*
1.25E15	9.90	1.04	0.0933	0.0398	0.583	0.602	0.120	0.338	0.417	0.115	1.13
1.35E15	9.86	1.12	0.111	0.0416	0.592	0.571	0.114	0.330	0.395	0.115	1.12
1.46E15	9.81	1.20	0.129	0.0434	0.601	0.540	0.107	0.322	0.372	0.113	1.11
1.58E15	9.74	1.27	0.148	0.0451	0.609	0.509	0.100	0.312	0.347	0.112	1.11
1.72E15	9.66	1.34	0.168	0.0468	0.617	0.479	0.0936	0.302	0.321	0.110	1.10
1.86E15	9.57	1.40	0.187	0.0486	0.624	0.450	0.0870	0.291	0.295	0.108	1.08
2.01E15	9.47	1.45	0.205	0.0503	0.631	0.421	0.0805	0.280	0.268	0.107	1.07
2.18E15	9.36	1.50	0.223	0.0520	0.638	0.394	0.0742	0.270	0.242	0.105	1.06
2.36E15	9.25	1.54	0.238	0.0537	0.644	0.368	0.0683	0.260	0.216	0.103	1.05
2.56E15	9.13	1.58	0.252	0.0553	0.649	0.344	0.0628	0.251	0.191	0.102	1.04
2.77E15	9.00	1.60	0.264	0.0570	0.654	0.321	0.0576	0.242	0.167	0.101	1.03
3.00E15	8.87	1.62	0.274	0.0586	0.659	0.300	0.0528	0.233	0.144	0.100	1.02
3.25E15	8.75	1.64	0.281	0.0601	0.663	0.280	0.0485	0.225	0.122	0.0995	1.01
3.52E15	8.62	1.65	0.286	0.0617	0.667	0.261	0.0445	0.218	0.100	0.0988	1.00
3.81E15	8.49	1.65	0.289	0.0632	0.670	0.244	0.0408	0.211	0.0797	0.0982	0.995
4.13E15	8.36	1.66	0.290	0.0647	0.673	0.228	0.0376	0.205	0.0601	0.0977	0.987

Table 2. Same as in Table 1, but for EOS AU.

	$\sim\epsilon^0$				$\sim\epsilon$		$\sim\epsilon^2$				
ρ_c (g cm^{-3})	R (km)	$M/M_\odot$	$E_B/M_\odot$	Ω^* (km^{-1})	R_g^*/R	ω_c^*/Ω^*	$\delta R^*/R$	$\delta M^*/M$	$\delta E_B^*/E_B$	$Q^*/(MR^2)$	e_s^*
7.62E14	10.3	0.602	0.0254	0.0285	0.513	0.763	0.150	0.322	0.461	0.0946	1.12
8.36E14	10.3	0.742	0.0413	0.0317	0.539	0.718	0.142	0.342	0.468	0.107	1.13
9.16E14	10.3	0.895	0.0632	0.0347	0.562	0.670	0.134	0.351	0.460	0.115	1.14
1.00E15	10.3	1.05	0.0914	0.0375	0.582	0.620	0.124	0.350	0.439	0.119	1.14
1.10E15	10.4	1.22	0.128	0.0402	0.601	0.566	0.112	0.342	0.406	0.120	1.13
1.21E15	10.4	1.40	0.175	0.0429	0.621	0.508	0.0989	0.327	0.361	0.120	1.12
1.32E15	10.4	1.57	0.229	0.0456	0.639	0.450	0.0850	0.310	0.311	0.119	1.10
1.45E15	10.3	1.72	0.285	0.0480	0.656	0.397	0.0716	0.291	0.260	0.118	1.08
1.59E15	10.3	1.84	0.338	0.0502	0.671	0.349	0.0594	0.273	0.210	0.118	1.06
1.74E15	10.2	1.94	0.383	0.0522	0.684	0.309	0.0489	0.258	0.165	0.118	1.04
1.91E15	10.1	2.01	0.421	0.0540	0.694	0.274	0.0399	0.244	0.124	0.118	1.03
2.09E15	9.94	2.06	0.451	0.0556	0.703	0.244	0.0323	0.232	0.0873	0.119	1.01
2.29E15	9.81	2.10	0.473	0.0573	0.711	0.217	0.0256	0.222	0.0533	0.120	1.00
2.51E15	9.68	2.12	0.488	0.0588	0.717	0.194	0.0199	0.213	0.0226	0.122	0.990
2.76E15	9.54	2.13	0.497	0.0602	0.722	0.174	0.0150	0.205	-0.00527	0.123	0.980
3.02E15	9.40	2.13	0.499	0.0616	0.727	0.156	0.0110	0.198	-0.0305	0.123	0.971

Table 3. Same as in Table 1, but for EOS FPS.

	$\sim \epsilon^0$				$\sim \epsilon$		$\sim \epsilon^2$				
ρ_c (g cm^{-3})	R (km)	$M/M_\odot$	$E_B/M_\odot$	Ω^* (km^{-1})	R_g^*/R	ω_c^*/Ω^*	$\delta R^*/R$	$\delta M^*/M$	$\delta E_B^*/E_B$	$Q^*/(MR^2)$	e_s^*
8.03E14	11.2	0.873	0.0533	0.0303	0.546	0.695	0.139	0.339	0.454	0.108	1.13
8.84E14	11.1	0.986	0.0704	0.0324	0.560	0.659	0.132	0.339	0.441	0.111	1.13
9.73E14	11.1	1.10	0.0901	0.0345	0.573	0.621	0.125	0.335	0.422	0.112	1.13
1.07E15	11.0	1.21	0.112	0.0364	0.585	0.584	0.117	0.328	0.399	0.112	1.12
1.18E15	10.9	1.31	0.135	0.0384	0.595	0.547	0.109	0.318	0.372	0.111	1.11
1.30E15	10.8	1.40	0.159	0.0403	0.605	0.512	0.101	0.308	0.344	0.109	1.10
1.43E15	10.7	1.48	0.183	0.0421	0.614	0.477	0.0935	0.296	0.315	0.107	1.09
1.57E15	10.6	1.56	0.206	0.0439	0.622	0.444	0.0861	0.285	0.286	0.105	1.08
1.73E15	10.5	1.62	0.227	0.0457	0.630	0.412	0.0790	0.273	0.256	0.103	1.07
1.91E15	10.3	1.67	0.247	0.0475	0.637	0.382	0.0721	0.261	0.227	0.102	1.05
2.10E15	10.1	1.71	0.264	0.0493	0.643	0.353	0.0657	0.250	0.198	0.0999	1.04
2.31E15	9.97	1.75	0.278	0.0510	0.649	0.327	0.0598	0.240	0.170	0.0985	1.03
2.54E15	9.80	1.77	0.289	0.0528	0.654	0.302	0.0543	0.230	0.144	0.0974	1.02
2.80E15	9.62	1.79	0.297	0.0545	0.658	0.279	0.0495	0.221	0.118	0.0964	1.01
3.08E15	9.45	1.80	0.301	0.0561	0.662	0.258	0.0451	0.213	0.0941	0.0955	0.999
3.39E15	9.28	1.80	0.303	0.0577	0.666	0.239	0.0413	0.206	0.0713	0.0947	0.990

Table 4. Same as in Table 1, but for EOS L.

	$\sim \epsilon^0$				$\sim \epsilon$		$\sim \epsilon^2$				
ρ_c (g cm^{-3})	R (km)	$M/M_\odot$	$E_B/M_\odot$	Ω^* (km^{-1})	R_g^*/R	ω_c^*/Ω^*	$\delta R^*/R$	$\delta M^*/M$	$\delta E_B^*/E_B$	$Q^*/(MR^2)$	e_s^*
2.35E14	14.9	0.362	0.00513	0.0127	0.426	0.886	0.173	0.234	0.396	0.0522	1.07
2.65E14	14.5	0.502	0.0119	0.0156	0.473	0.853	0.164	0.302	0.459	0.0804	1.11
3.00E14	14.5	0.680	0.0242	0.0182	0.510	0.812	0.159	0.350	0.500	0.105	1.14
3.39E14	14.6	0.896	0.0445	0.0206	0.540	0.765	0.153	0.377	0.517	0.122	1.16
3.83E14	14.8	1.14	0.0751	0.0228	0.564	0.711	0.144	0.387	0.510	0.132	1.17
4.33E14	15.0	1.40	0.116	0.0249	0.585	0.655	0.134	0.383	0.485	0.135	1.16
4.89E14	15.1	1.67	0.168	0.0268	0.603	0.597	0.121	0.370	0.448	0.133	1.15
5.53E14	15.1	1.91	0.229	0.0286	0.619	0.540	0.108	0.351	0.402	0.130	1.14
6.24E14	15.1	2.14	0.292	0.0303	0.633	0.486	0.0955	0.330	0.353	0.126	1.12
7.06E14	15.0	2.32	0.353	0.0319	0.645	0.437	0.0834	0.309	0.304	0.122	1.10
7.97E14	14.8	2.46	0.407	0.0334	0.656	0.393	0.0727	0.290	0.259	0.118	1.08
9.01E14	14.6	2.56	0.450	0.0348	0.664	0.355	0.0636	0.273	0.218	0.116	1.06
1.02E15	14.4	2.64	0.483	0.0361	0.671	0.322	0.0560	0.258	0.182	0.113	1.05
1.15E15	14.2	2.68	0.504	0.0373	0.676	0.294	0.0498	0.246	0.151	0.111	1.03
1.30E15	13.9	2.70	0.514	0.0383	0.679	0.271	0.0449	0.235	0.125	0.110	1.02
1.47E15	13.7	2.70	0.517	0.0393	0.682	0.251	0.0411	0.226	0.102	0.108	1.01

Table 5. Same as in Table 1, but for EOS APRb.

	$\sim\epsilon^0$				$\sim\epsilon$		$\sim\epsilon^2$				
ρ_c (g cm^{-3})	R (km)	$M/M_\odot$	$E_B/M_\odot$	Ω^* (km^{-1})	R_g^*/R	ω_c^*/Ω^*	$\delta R^*/R$	$\delta M^*/M$	$\delta E_B^*/E_B$	$Q^*/(MR^2)$	e_s^*
6.16E14	12.1	0.654	0.0243	0.0234	0.497	0.771	0.152	0.294	0.430	0.0835	1.10
6.78E14	11.9	0.776	0.0368	0.0261	0.518	0.733	0.145	0.311	0.438	0.0927	1.11
7.46E14	11.8	0.917	0.0546	0.0288	0.539	0.691	0.137	0.322	0.436	0.100	1.12
8.21E14	11.7	1.07	0.0787	0.0315	0.559	0.644	0.128	0.326	0.423	0.105	1.12
9.04E14	11.6	1.24	0.110	0.0341	0.578	0.594	0.118	0.324	0.400	0.108	1.12
9.95E14	11.6	1.40	0.147	0.0366	0.596	0.543	0.107	0.316	0.369	0.109	1.11
1.10E15	11.5	1.56	0.190	0.0390	0.613	0.492	0.0953	0.305	0.331	0.109	1.10
1.21E15	11.4	1.70	0.236	0.0413	0.629	0.443	0.0837	0.291	0.289	0.109	1.08
1.33E15	11.3	1.83	0.282	0.0435	0.643	0.397	0.0724	0.276	0.247	0.108	1.07
1.46E15	11.1	1.94	0.325	0.0456	0.656	0.355	0.0619	0.262	0.204	0.108	1.05
1.61E15	11.0	2.02	0.365	0.0475	0.668	0.316	0.0522	0.248	0.162	0.108	1.03
1.77E15	10.8	2.09	0.398	0.0494	0.678	0.281	0.0435	0.235	0.123	0.108	1.02
1.95E15	10.6	2.14	0.425	0.0512	0.688	0.250	0.0359	0.224	0.0865	0.109	1.01
2.15E15	10.5	2.17	0.444	0.0529	0.695	0.223	0.0292	0.214	0.0525	0.110	0.993
2.36E15	10.3	2.19	0.457	0.0545	0.702	0.199	0.0235	0.205	0.0212	0.111	0.981
2.60E15	10.1	2.20	0.463	0.0560	0.707	0.178	0.0187	0.198	-0.00756	0.112	0.971

Table 6. Properties of HT models matching the slowest rotating CST models listed in Tables 1-5 of BS. For each EOS, on top we present matching models for the $M = 1.4M_\odot$ ('14') sequence; separated by an horizontal line, we give matching models for the maximum-mass ('MM') sequence. From left to right we list: the central energy density $\bar{\rho}_c$ for which we find a matching solution (if such a central energy density exists); the value of $\epsilon = \bar{J}/J^*$ at the given central energy density; the gravitational mass $\bar{M}$ and the angular momentum $\bar{J}$, in geometrical units; the value of the quadrupole moment predicted by the HT equations of structure, $Q^{\rm HT}$, in geometrical units; the percentage deviation of the HT quadrupole moment from its value Q for the CST spacetime.

EOS	$\bar{\rho}_c$ (g cm^{-3})	ϵ	$\bar{M}$ (km)	$\bar{J}$ (km^2)	$Q^{\rm HT}$ (km^3)	δQ (%)
A 14	1.8110E15	0.23236	2.0729	0.8121	1.1053	10.4
	1.7238E15	0.40060	2.0800	1.3267	3.2644	22.9
	1.6152E15	0.55642	2.0870	1.7037	6.2084	41.8
	1.4476E15	0.76898	2.0940	2.0220	11.372	84.2
A MM	3.4253E15	0.19954	2.4519	0.9857	0.7192	15.4
	3.0369E15	0.32653	2.4608	1.5731	2.0107	21.3
	2.6524E15	0.46715	2.4726	2.1471	4.2850	32.4
	2.2177E15	0.65300	2.4870	2.7173	8.6795	59.7
AU 14	1.1916E15	0.24345	2.0734	0.8704	1.5633	10.4
	1.1666E15	0.40245	2.0794	1.3551	4.1490	23.3
	1.1217E15	0.59998	2.0868	1.7984	8.6917	49.4
	1.0426E15	0.87088	2.0925	2.0808	16.160	109.8
AU MM	2.5557E15	0.21819	3.1645	1.9389	1.6913	23.5
	2.2777E15	0.36512	3.1838	3.1382	4.7843	29.3
	2.0247E15	0.51420	3.2068	4.1755	9.4664	40.5
	1.7585E15	0.69420	3.2302	5.0587	16.844	66.1
FPS 14	1.2642E15	0.25144	2.0720	0.8722	1.6662	10.2
	1.2195E15	0.39258	2.0769	1.2971	4.0094	21.1
	1.1565E15	0.54440	2.0825	1.6649	7.5270	39.0
	1.0626E15	0.74208	2.0881	1.9766	13.279	74.8
FPS MM	2.8003E15	0.20109	2.6648	1.1604	0.9524	14.7
	2.4765E15	0.32814	2.6740	1.8467	2.6577	20.8
	2.1574E15	0.46924	2.6864	2.5193	5.6832	32.1
	1.7968E15	0.65491	2.7014	3.1853	11.536	59.7
L 14	4.2540E14	0.25862	2.0717	0.9726	4.0544	10.4
	4.1435E14	0.43170	2.0760	1.5007	10.756	27.1
	3.9803E14	0.61954	2.0802	1.8991	20.412	54.6
L MM	1.2480E15	0.18716	4.0130	2.5589	3.0214	13.8
	1.0717E15	0.32762	4.0297	4.3607	9.6976	21.0
	9.2990E14	0.47634	4.0515	6.0142	21.145	34.0
	7.8669E14	0.66069	4.0754	7.4955	41.295	63.6
APRb 14	9.7905E14	0.27032	2.0753	0.9349	2.1641	10.1
	9.6661E14	0.35913	2.0781	1.2034	3.7615	17.4
	9.5231E14	0.44237	2.0810	1.4276	5.6017	25.5
	9.3547E14	0.52688	2.0838	1.6238	7.7629	35.6
	9.1459E14	0.62069	2.0866	1.8017	10.442	49.1
APRb MM	2.4553E15	0.17324	3.2640	1.6051	1.1343	25.3
	2.3001E15	0.24355	3.2705	2.2296	2.2707	23.0
	2.0765E15	0.36617	3.2864	3.2541	5.2083	28.3
	1.8261E15	0.52120	3.3086	4.3615	10.632	39.8
	1.6702E15	0.63017	3.3232	4.9670	15.494	54.0
	1.4393E15	0.81746	3.3393	5.5922	25.448	94.7